Fermi National Accelerator Laboratory

FERMILAB-Conf-85/29-T
February, 1985

The Last Hurrah For Quarkonium Physics:

The Top System

E. Eichten

Fermi National Accelerator Laboratory
P.O. Box 500
Batavia, Illinois 60510

Lectures presented at the 1984 SLAC Summer School

Contents:

I. INTRODUCTION

This year marks the tenth anniversary of the discovery of the J/ψ. During this time much experimental data and theoretical understanding has been accumulated for heavy quark systems.

Heavy quark systems have a very clean spectroscopy which allows precision measurements of all the basic properties of the states (mass, spin, parity, and charge conjugation), as well as transition and decay rates. In particular, the analysis of the observed spectrum of $(c\bar{c})$ and $(b\bar{b})$ resonances shown in Figure 1 has provided important insight into the physics of heavy quark-antiquark (quarkonium) systems. In addition to these systems, the low-lying states with the associated new flavor (i.e. one heavy quark and one light quark system) have been observed for the $(c\bar{u})$, $(c\bar{d})$, $(c\bar{s})$, $(b\bar{u})$, and $(b\bar{d})$ systems.

From a theoretical point of view heavy quark systems are interesting because they are relatively simple systems. To a good approximation the quark motion in these bound states should be nonrelativistic. For the ground state of a $(Q\bar{Q})$ system we may determine the conditions under which the system will be nonrelativistic by a simple application of the Virial Theorem and the Uncertainty Principle.

The average kinetic energy of the system, $\langle K.E.\rangle$, is related to the potential energy via the Virial Theorem:

$$\langle K.E.\rangle = \langle \frac{p^2}{2m} \rangle = \frac{1}{2} \langle R \frac{dV}{dR} \rangle \qquad (1.1)$$

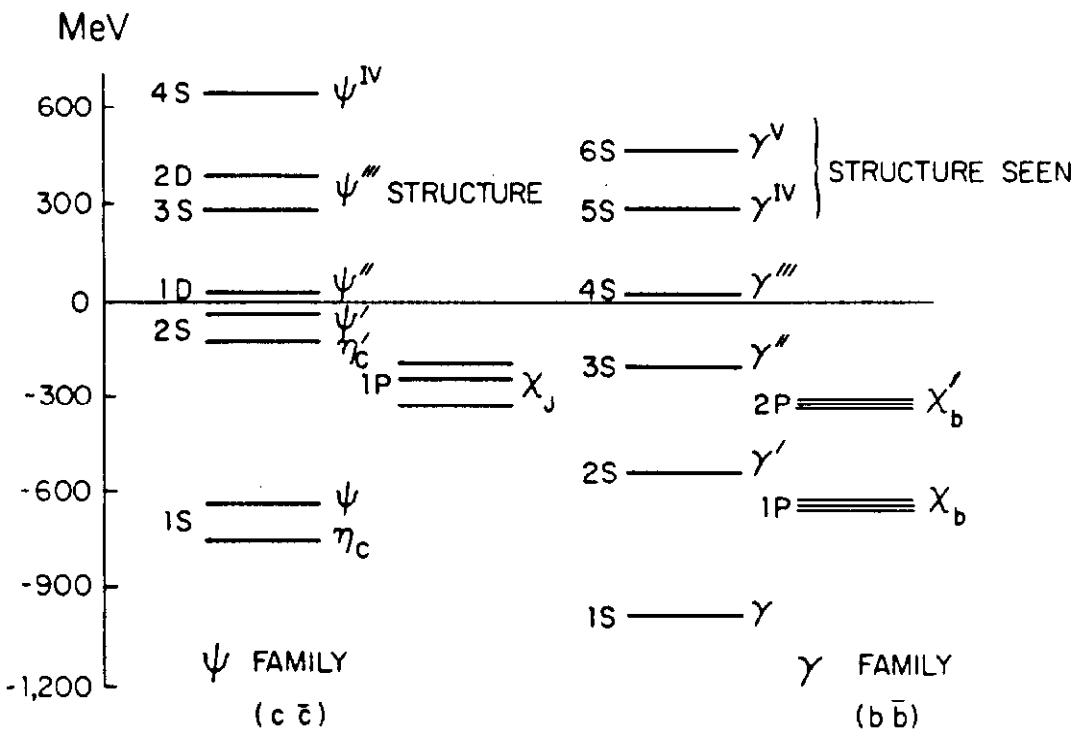

Figure 1: The experimentally observed spectrum for the ($c\bar{c}$) and ($b\bar{b}$) systems. Above threshold for Zweig allowed decays the association between structure in R and potential model states is provisional. This is especially true for the ($b\bar{b}$) system.

and by the Uncertainty Principle $\langle R^2\rangle^{1/2} \times \langle p^2\rangle^{1/2} \geq \hbar$. Hence

$$\left\langle \frac{v^2}{c^2} \right\rangle^{1/2} \sim \frac{1}{\hbar c} \left\langle R^2 \frac{dV}{dR} \right\rangle . \tag{1.2}$$

In Q.E.D. $\langle v^2/c^2\rangle^{1/2} \approx \alpha Z$ where Z is the change of the nucleus; therefore the system is nonrelativistic for $\alpha Z \ll 1$ independent of the reduced mass of the system. The situation for Q.C.D. is more complicated. If $V(R) = AR^\beta$ then $\langle R^2\rangle^{1/2} \sim (m\beta A)^{-1/(2+\beta)}$; and there will be some threshold value of the reduced mass, m, for which the system would be expected to be nonrelativistic. For large R, we expect $V(R) = KR$ where K is the string tension ($\approx (400\ \text{MeV})^2$). Thus, for example, $\langle v^2/c^2\rangle^{1/2} \lesssim 0.5$ requires a heavy quark mass $m_Q (=2m)$ greater than about 1 GeV.

Within the standard electroweak model with three generations of quarks and leptons there remains only one missing element -- the top quark. In my lectures I will apply what is known about heavy quark systems to the top system -- both toponium and open top. Many properties of these systems can be predicted. I will also discuss what can be learned from toponium about quarkonium physics under realistic experimental conditions. Section 2 contains a discussion of the spectrum of toponium states: the expected excitation spectrum, the implications for probing the heavy quark potential, and an estimate of the fine and hyperfine splittings. Section 3 contains a discussion of production and decay properties. In particular, the growing importance of electroweak effects on the decays of toponium states is emphasized. The properties of the

low-lying open top mesons are also discussed. Section 4 is devoted to consideration of some more exotic possibilities for the top system. In particular, three possibilities are considered: (1) The influence of light charged or neutral Higgs-like scalars on toponium decays; (2) Possible direct production of $J = 1$ $(t\bar{t})$ P-states via the axial vector coupling of the Z^0 to $(t\bar{t})$; and (3) Toponium -- Z^0 interference effects which would result if the mass difference between some toponium resonance and the Z^0 were less than the width of the Z^0.

In the remainder of this introductory section I will discuss the present situation for the nonrelativistic potential between heavy quarks. For a particularly clear general review of the theory of heavy quark systems -- potentials, spin dependent forces, and hadronic transitions -- I refer the reader to the 1983 SLAC Summer School Lectures by M. Peskin.[1] In my lectures I will assume the reader is familiar with this material and will restrict my discussion of theoretical issues to recent developments.

The Nonrelativistic Potential

For small R (<.1 fm), the heavy quark potential can be calculated in Q.C.D. perturbation theory. The leading behavior of the result can be expressed in momentum space as:[2,3]

$$V(\vec{Q}^2) = -\frac{4}{3}\,4\pi\alpha_s(\vec{Q}^2)/\vec{Q}^2 \qquad (1.3)$$

where $\vec{Q}$ = momentum conjugate to $\vec{R}$. The running coupling $\alpha_s(\vec{Q}^2)$ is

given by:[4]

$$\alpha_s(\vec{Q}^2) \underset{\vec{Q}^2\to\infty}{\sim} \frac{4\pi}{b_0 \ln(\vec{Q}^2/\Lambda^2)} - \frac{4\pi b_1}{b_0^3} \frac{\ln\left(\ln(\vec{Q}^2/\Lambda^2)\right)}{\left(\ln(\vec{Q}^2/\Lambda^2)\right)^2} + O\left(\frac{1}{\left(\ln(\vec{Q}^2/\Lambda^2)\right)^3}\right) . \tag{1.4}$$

where $b_0 = 11 - 2/3N_f$ and $b_1 = 102 - 10N_f - 8/3N_f$. N_f is the number of effective quark flavors (N_f=4 for the top system). Λ is the scale parameter for the minimum subtraction-bar renormalization scheme.

This expression can be transformed to position space,[5] to obtain:

$$V^{Q.C.D.}(R) \underset{R\to 0}{\sim} -\frac{4}{3}\frac{\alpha_s(R)}{R} \tag{1.5}$$

where

$$\alpha_s(R) \underset{R\to 0}{\sim} \left[\frac{4\pi}{b_0 \ln(1/R^2\Lambda^2)}\right]\left\{1 - \frac{b_1}{b_0^2}\frac{\ln\left[\ln(1/R^2\Lambda^2)\right]}{\ln(1/R^2\Lambda^2)} + B/\ln(1/R^2\Lambda^2) + \ldots\right\} \tag{1.6}$$

and

$$B = \frac{1}{b_0}\left[\frac{31}{3} - \frac{10}{9}N_f\right] + 2\gamma_E$$

and γ_E is the Euler constant (~.5772). Unfortunately for the ($c\bar{c}$) and ($b\bar{b}$) systems we require knowledge of the potential outside the region of validity of perturbation theory. This larger R region can

be studied numerically using lattice methods as I will discuss below, however so far no analytic methods exist. The result has been a wide variety of phenomenological potentials.

The phenomenological potentials can be separated into two broad categories. The first category incorporates to some approximation the expected behavior of Q.C.D. at short distance ($-4/3\ \alpha_s(R)/R$) and long distance (KR). Two simple examples of this type are:

(1) Cornell Model:[6]

$$V(R) = -K/R + R/a^2 + C \tag{1.7}$$

where $K = .48$, $a = 2.34(\text{GeV})^{-1}$, and $C = -.25$ GeV ;

and

(2) Richardson's Model:[7]

$$V(R) = \int \frac{d^3Q}{(2\pi)^3}\, e^{i\vec{Q}\cdot\vec{R}} \left[-\frac{4}{3}\,\frac{12\pi}{27}\,\frac{1}{\vec{Q}^2 \ln(1+\vec{Q}^2/\Lambda^2)} \right] + C \tag{1.8}$$

where $\Lambda = .398$ GeV and $C = 0.0$ (input).

The second category is motivated purely by the data on $(c\bar{c})$ and $(b\bar{b})$ systems. Two simple models are motivated by the approximate equality of the $\Upsilon'-\Upsilon$ and the $\psi'-\psi$ mass difference. For a potential of the form $V(R) = AR^\beta$ the nonrelativistic Schroedinger Equation can be reexpressed in a form independent of m_Q and dependent only on $\rho = \xi R$ and $\epsilon = E/(2m_Q)\xi^2$ where $\xi = (Am_Q)^{1/(2+\beta)}$. Hence, if E_n is the energy of the nth excited state, then for any simple power law (scaling) potential $(E_{n_1}-E_{n_2})/(E_{n_3}-E_{n_4})$ is independent of m_Q. Mass independent spacing requires $\beta \simeq 0$. Two specific potentials which

exhibit this behavior are:

(3) Power Law:[8]

$$V(R) = A(R/R_0)^{\beta} + C \tag{1.9}$$

where A = 5.82 GeV, $R_0 = 1(\text{GeV})^{-1}$, $\beta = .104$, and C = -6.377 GeV.

(4) Logarithmic Model:[9]

$$V(R) = A \ln(R/R_0) + C \tag{1.10}$$

where A = .70 GeV, $R_0 = 2.0(\text{GeV})^{-1}$, and C = -.121 GeV.

Fitting the parameters using the $(b\bar{b})$ system, all four of these potentials fit the gross spectrum of the $(c\bar{c})$ system very well. This is less surprising than it might first appear. When one adds the overall constant (C) to the potentials so that they agree at R=.4 fm and then plots the potentials fitted to the $(b\bar{b})$ system in the same figure, one finds all these potentials are in remarkable numerical agreement within the region .1 fm $\leq$ R $\leq$ 1 fm (See Figure 2). Since the RMS radius of each of the $(c\bar{c})$ and $(b\bar{b})$ states below threshold for Zweig allowed decays is in this range of R, the agreement of the predictions of these various potentials is easily understood.

Another popular approach has been to use the inverse scattering method[10] to determine the potential directly from the data. The potential so determined agrees well with those shown in Figure 2. Furthermore, the potential constructed from the data in the $(c\bar{c})$ system agrees well with that constructed from the data in the $(b\bar{b})$ system.[11] This supports the expectation in Q.C.D. of the flavor independence of the potential.

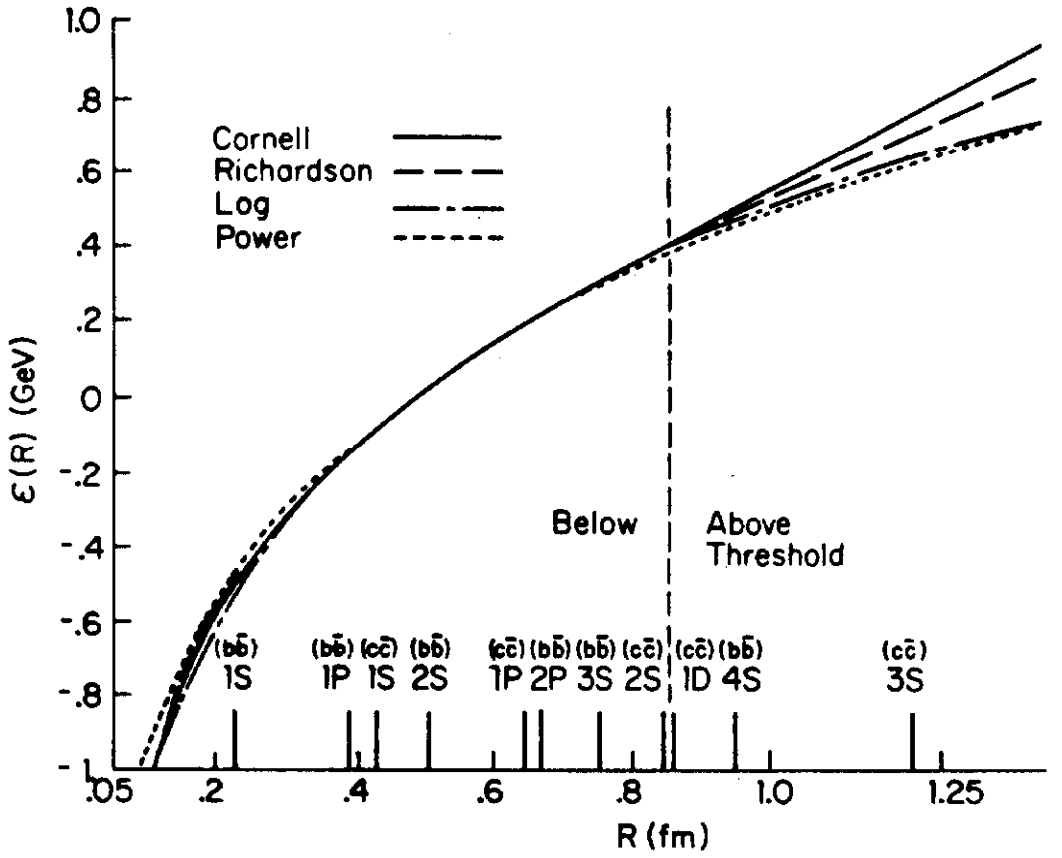

Figure 2: Phenomenological potentials for the $(Q\bar{Q})$ system. The RMS radii of the observed $(c\bar{c})$ and $(b\bar{b})$ states are indicated by markers.

From the phenomenological considerations we have obtained a well defined potential for .1 fm < R < 1. fm. How does this potential agree with Q.C.D.?

There can be no complete answer to this question at the present time; however, numerical studies of the interquark potential have been done using the lattice formulation of Q.C.D.[12] For example, the results of a recent study by S. Otto and J. Stack[13] are shown in Figure 3. Before comparing these results with the phenomenological potential a few words of caution are necessary. Most importantly, the present lattice calculations are done in the quenched approximation (i.e., in the absence of internal light quark loops). The effects of quark loops (or equivalently coupling to real and virtual hadronic decay channels) will certainly modify the effective potential between the heavy quarks. The result of the Cornell Group's work on the effects of coupling to decay channels on the effective potential in the $(c\bar{c})$ system[6] suggests that these effects on the parameters of the potential are of the order of 10-20% for R in the range of .1 to 1. fm. Another important caveat is that the size of the systematic errors in lattice calculations is not very accurately known yet. The simplest way to compare the lattice potential with the phenomenological potentials is to note that the logarithmic model gives a good fit in the range of R probed by the $(c\bar{c})$ and $(b\bar{b})$ systems; hence plotting $V/\sqrt{K}$ versus $\ln(\sqrt{K}R)$ should give an approximate straight line for a wide range of R. The result of doing this plot is shown in Figure 4. The agreement is clearly good.

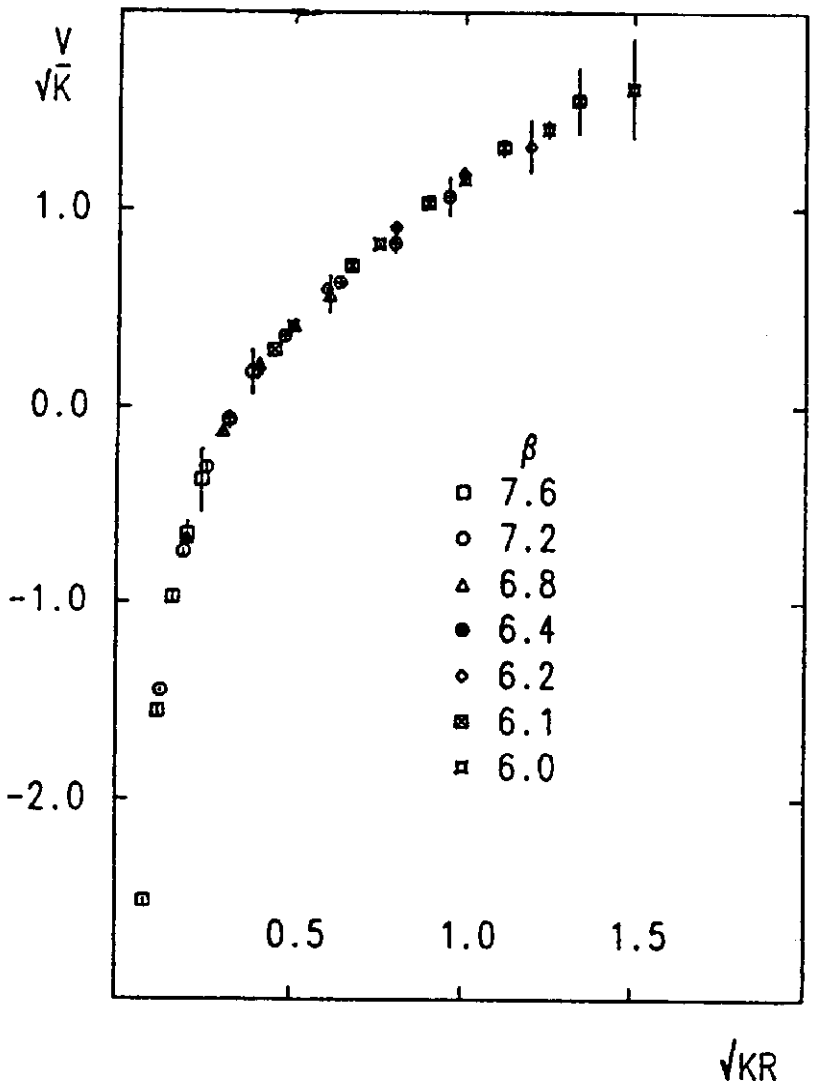

Figure 3: The SU(3) Heavy Quark Potential determined on a 12 × 12 × 12 × 16 lattice. No internal light quark loops have been included. K is the Q.C.D. string tension. From Ref. 13.

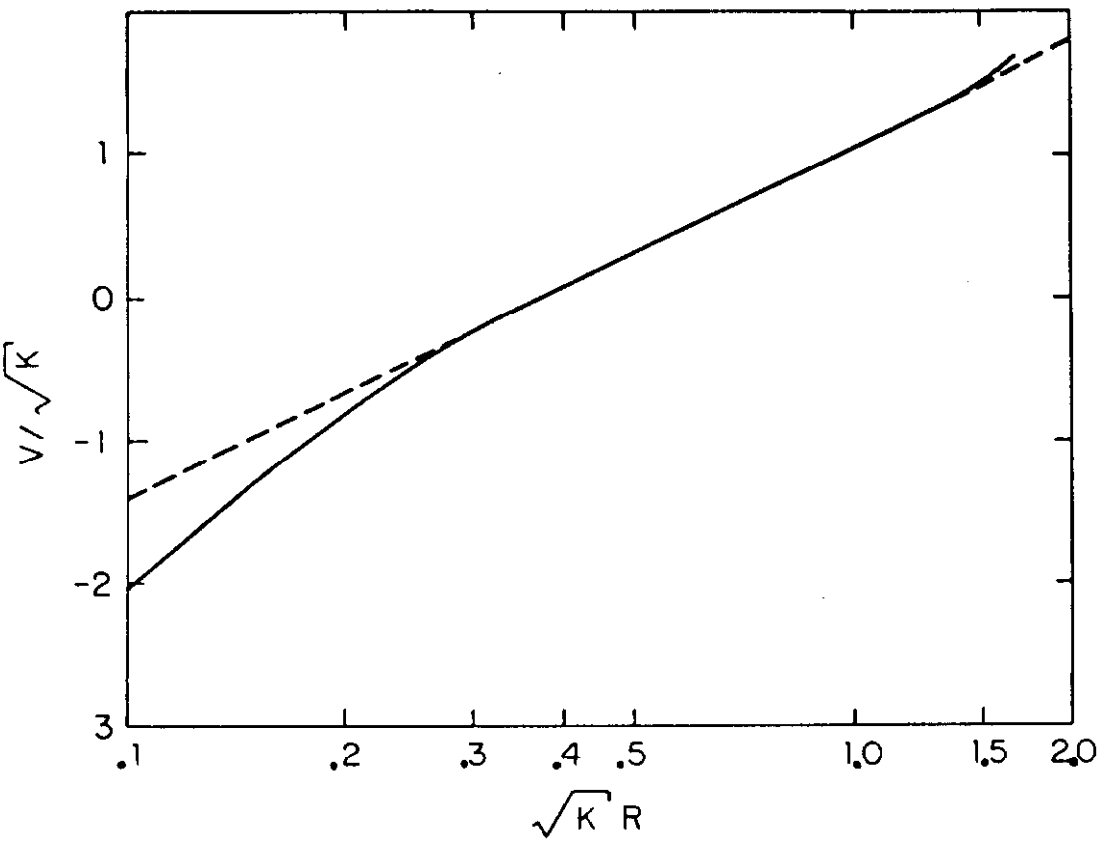

Figure 4: Comparison of a fit to the Lattice Potential of Fig. 3 (solid curve) with a logarithmic form (dotted straight line).

If we attempt to compare the lattice potential with the phenomenological potentials numerically, the physical value of the string tension, K, is required. The hadronic string tension is expected to have a value around $(400\ \text{MeV})^2$. If this value is used the potentials can be compared directly. The comparison with $\sqrt{K} = 400$ MeV for the Cornell Model is shown in Figure 5. It is interesting to adjust the value of $\sqrt{K}$ to obtain the best fit (at large R) for the Cornell Model since it is expected to have the proper Q.C.D. behavior at large R. The resulting value is $\sqrt{K} = 480$ MeV. The comparison of the lattice potential with $\sqrt{K} = 480$ MeV for both the Cornell and Richardson's Model is shown in Figure 6. The agreement is quite good.

Other lattice calculations[14] have determined that $\Lambda_{Lattice}/\sqrt{K} = 9.63 \times 10^{-3}$. Using this result and the relation between $\Lambda_{Lattice}$ and $\Lambda_{\overline{MS}}$:[15]

$$\Lambda_{Lattice} = 1./38.8\ \Lambda_{\overline{MS}} \quad . \tag{1.11}$$

We can convert the measurement of $\sqrt{K}$ provided by the phenomenological heavy quark potentials into a measurement of $\Lambda_{\overline{MS}}$;

$$\Lambda_{\overline{MS}} = 180\ \text{MeV} \quad . \tag{1.12}$$

A phenomenologically acceptable value.

To summarize the present situation with regard to the nonrelativistic potential for heavy quark - antiquark systems:

(1) The potential is known very accurately in the range .1 fm $\lesssim$ R $\lesssim$ 1 fm. All the phenomenological potentials are

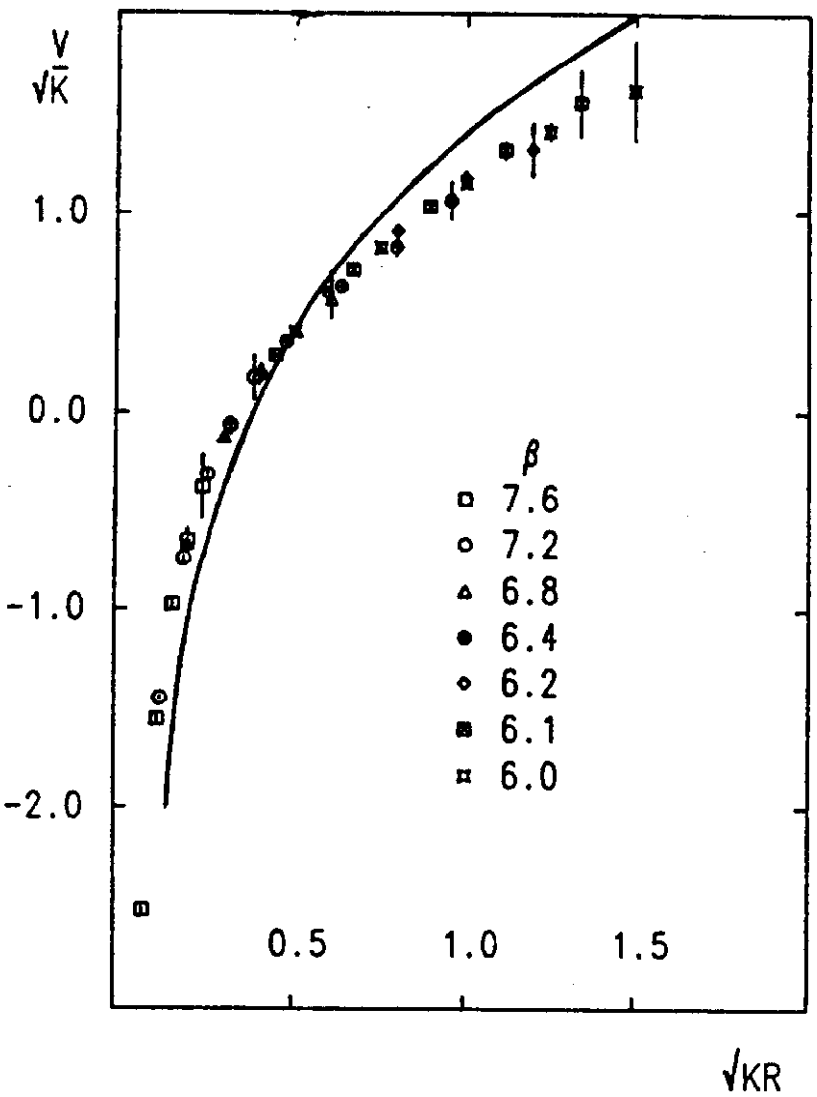

Figure 5: Comparison of the Cornell Model potential with the lattice result of Fig. 3. Here √K = 400 MeV.

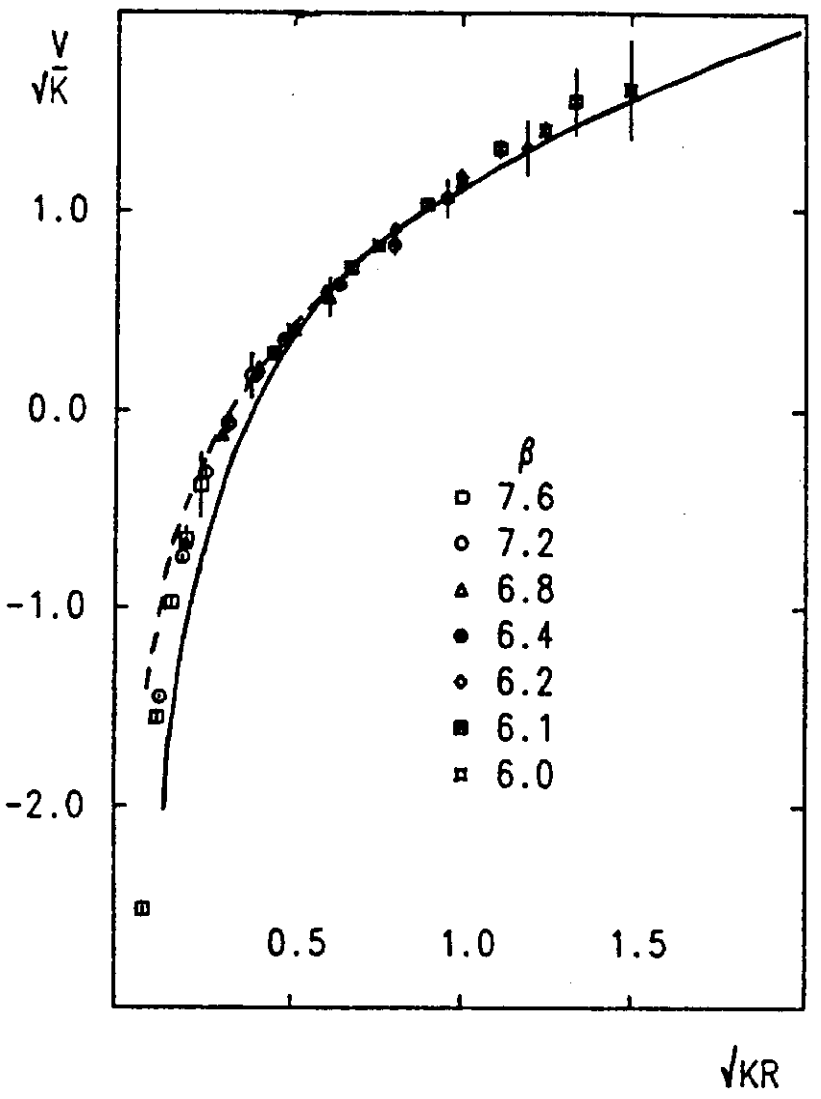

Figure 6: Comparison of both the Cornell Model (solid line) and Richardson's Model (dashed line) with the lattice results. Here √K = 480 MeV.

essentially identical (numerically) in this region. Remaining differences in this range are small compared to the relativistic corrections which have not been incorporated in this analysis.

(2) For R<.1 fm the phenomenological potentials differ significantly, but Q.C.D. perturbation theory dictates the correct form.

(3) The flavor independence of the potentials has been tested by the agreement of the potentials fitted to the $(b\bar{b})$ system with the spectrum of the $(c\bar{c})$ states and model independently by the inverse scattering method.

(4) The interquark potential in Q.C.D. determined by lattice methods is in good agreement with the phenomenological potentials discussed here.

We can conclude from (1)-(4) above that the nonrelativistic potential is well determined and flavor independent for R<1 fm. For larger distances the effects of open channels cannot be ignored.[16]

II. TOPONIUM SPECTROSCOPY

The nonrelativistic potential provides a simple and reliable model of heavy $(Q\bar{Q})$ physics for the $(b\bar{b})$ and $(c\bar{c})$ systems. How will the top system fit into this framework?

It should be clear that the nonrelativistic approximation should be even better for the $(t\bar{t})$ than for the $(b\bar{b})$ system since the mass of the top quark must be at least[17]

$$m_t \gtrsim 22.7 \text{ GeV} \tag{2.1}$$

The best upper bound on the top quark mass arises from the requirement that the top quark does not renormalize low energy electroweak observables more than consistent with experiment uncertainties. In particular,

$$\rho \equiv \frac{M_W^2}{M_Z^2(1-x_W)} \simeq 1. + \frac{3G_F m_t^2}{8\pi^2\sqrt{2}} \tag{2.2}$$

where $m_t >> m_b$. A recent compilation by Marciano and Sirlin[18] of neutral-current cross-section measurements yields a value

$$\rho = 1.02 \pm .02 \tag{2.3}$$

This suggests a bound

$$m_t < 350 \text{ GeV} \tag{2.4}$$

for the top quark mass.

Recently, the UA1 Collaboration[19] has announced preliminary evidence for the top quark, with 30 GeV$\leq m_t \leq$60 GeV. I will focus my discussion on this mass range for top and will use the median value 45 GeV when required to use a particular mass in the discussion. As we shall see, this mass range is also very interesting theoretically as it is a transitional region between standard quarkonium physics for lower masses and the dominance of electroweak physics for higher masses.

To begin the discussion of toponium spectroscopy, consider the impact the top system will have on our knowledge of the

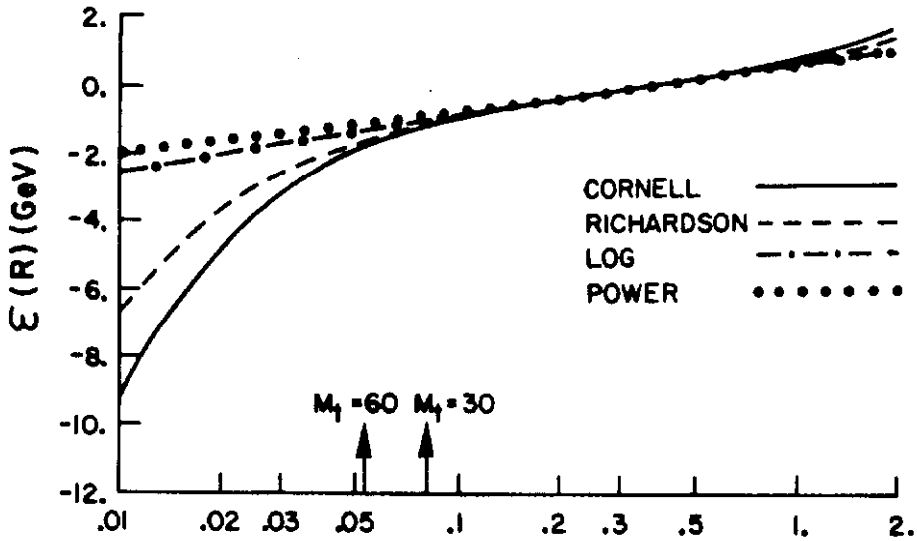

Figure 7: The short distance behaviour of the various ($Q\bar{Q}$) potentials of Fig. 2. The horizontal axis is the distance R (in fm) on a logarithmic scale. The markers indicate the RMS radius of the 1^3S_1 ($t\bar{t}$) state for m_t = 30 GeV and m_t = 60 GeV.

nonrelativistic potential. The ground state 1^3S_1 $(t\bar{t})$ state has a RMS radius of approximately .06 fm for m_t=45 GeV. In this region of R the various phenomenological potentials differ considerably. The short distance behavior of the four potentials we have discussed is shown in Figure 7. It is clear from the figure that it will be easy to distinguish the short distance behavior predicted by Q.C.D. (incorporated in Richardson's Model) from other potential forms.

One simple quantity which shows the sensitivity of the toponium system to the short range piece of the potential is the mass difference between the 2^3S_1 and 1^3S_1 $(t\bar{t})$ states. This mass difference is shown for various potentials in Figure 8. In as much as Richardson's potential has the correct short distance behavior, we must conclude that all other potentials which do not have this behavior will fail badly in describing the properties of the low-lying $(t\bar{t})$ states. Two conclusions follow immediately: (1) Simple scaling arguments[20] for the dependence of observables on m_Q (which work well in going from the $(c\bar{c})$ to $(b\bar{b})$ systems) will generally fail in going from the $(b\bar{b})$ to $(t\bar{t})$ systems; and (2) The difference between a potential which has a fixed coupling strength for the Coulomb contribution (e.g. the Cornell Model) and one with a running coupling as expected in Q.C.D. (e.g. Richardson's Model) is significant.

It has been suggested[21] that we may use the strong dependence of the properties of the low-lying toponium spectrum to directly measure $\alpha_s(R)$ and in this way extract a measurement of $\Lambda_{\overline{MS}}$ in Q.C.D. As seen in Figure 8, the splittings of low-lying toponium are in

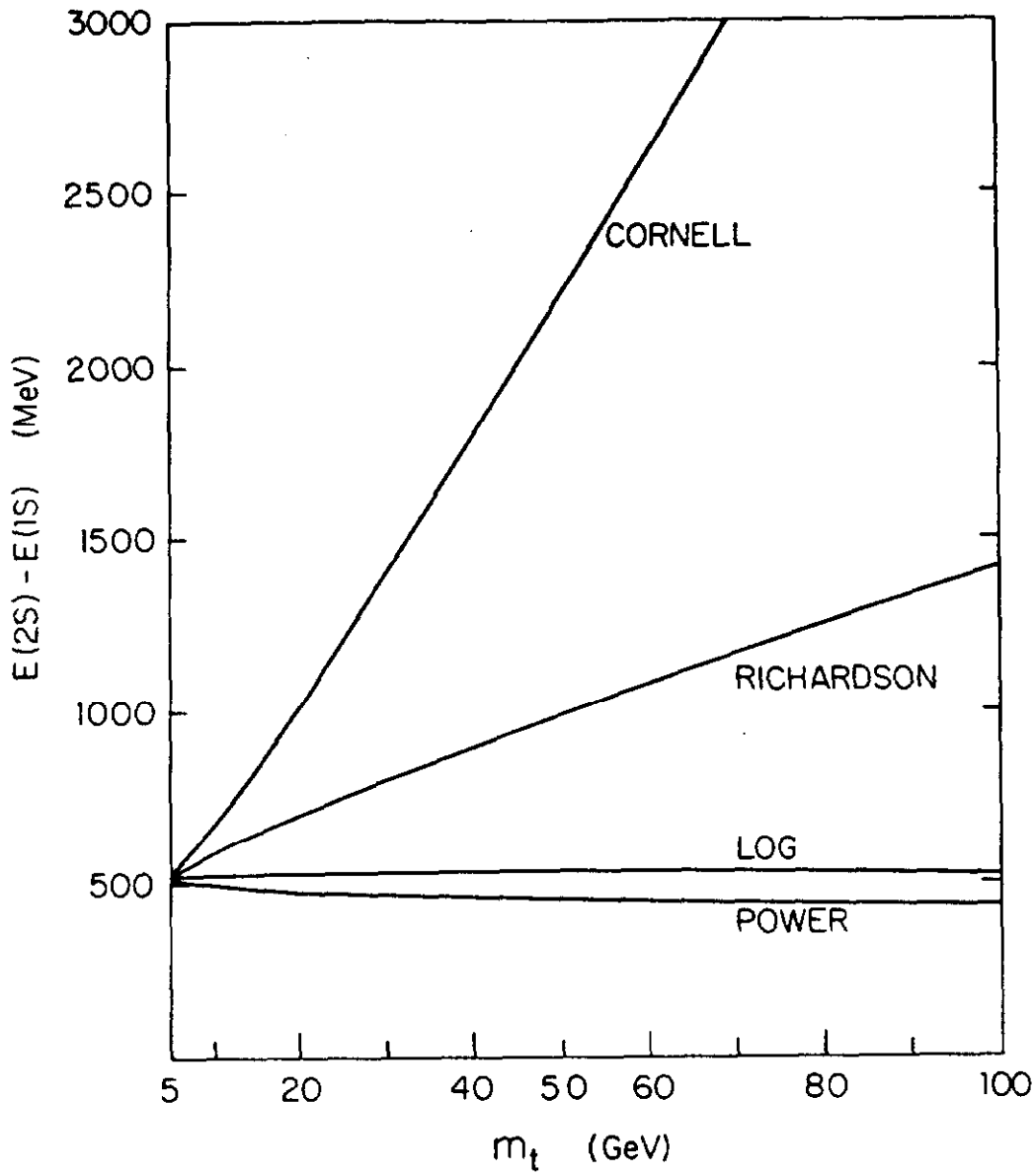

Figure 8: The 2S-1S energy splitting for the various potentials of Fig. 2 plotted as a function of top quark mass m_t.

fact quite sensitive to the running of $\alpha_s(R)$ given via Eq. (1.6). However for top quark masses less than $\approx$100 GeV/c^2 even the ground state is still sensitive to the intermediate distance (R>.1 fm) behavior of the potential and thus does not provide a clean test of perturbative Q.C.D.[22] To see this consider the potential given in Q.C.D. perturbation theory as R$\to$0 given by Eqs. (1.5) and (1.6). The comparison of this potential for various values of $\Lambda_{\overline{MS}}$ with Richardson's potential is shown in Figure 9. As R increases the perturbative potential becomes unreliable; and it is necessary to cutoff the large R behavior in some way. But if the properties of the state were determined by the sufficiently short distance behavior, this cutoff would be immaterial. (Assuming of course that the potential increases monotonically for all R.) For explicit comparison I will choose to stop the running of $\alpha_s(R)$ when $\alpha_s(R)$=.5. It is clear that without the long range confining feature of Richardson's potential the wavefunction would extend to larger distance; hence the RMS radius and the wavefunction at the origin of the ground state 1^{--} ($t\bar{t}$) system should be sensitive to remaining effects of nonperturbative contributions to the potential. Comparing results for various potentials we have:

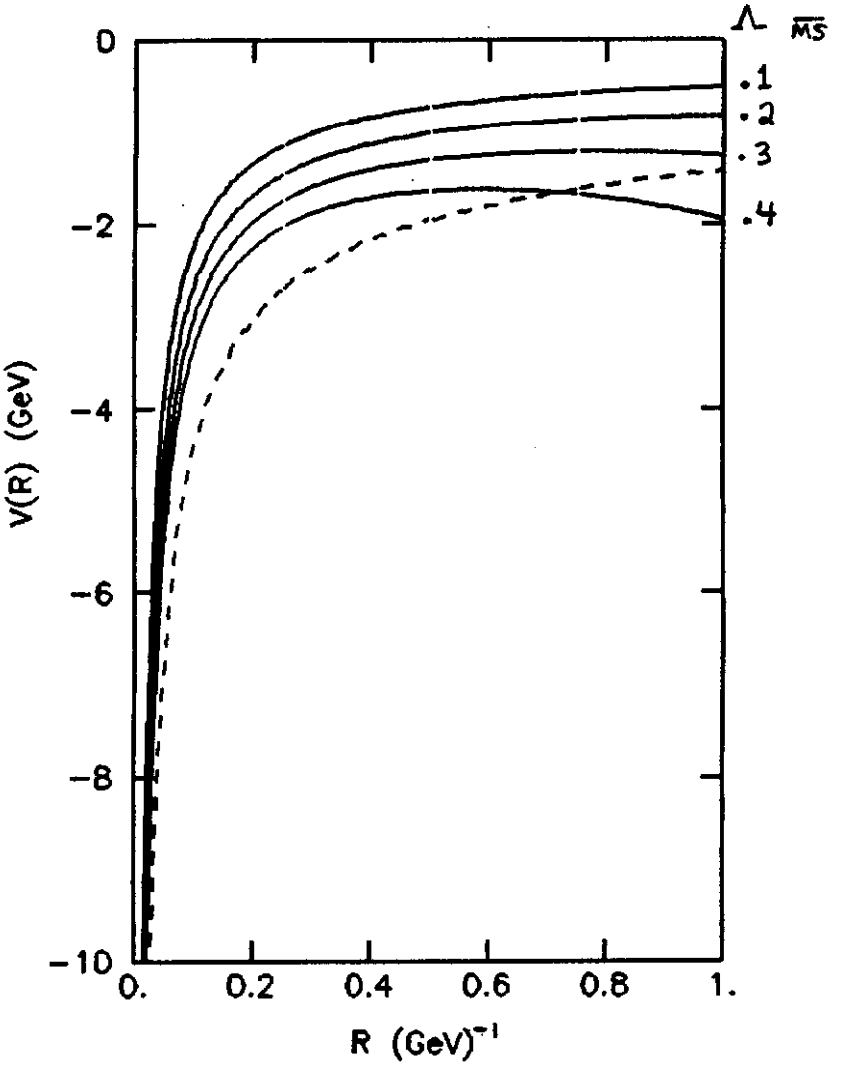

Figure 9: Comparison of Richardson's potential (dashed curve) with the potential (solid curve) given by perturbative Q.C.D. in Eqs. (1.5) and (1.6) for various values of $\Lambda_{\overline{MS}}$ ($\Lambda_{\overline{MS}}$ = 0.1, 0.2, 0.3, and 0.4 GeV).

Potential	$\langle R^2 \rangle^{1/2}$ (fm)	$\Gamma_0^{e^+e^-}$ (keV)
Richardson	.058	8.5
Q.C.D. Λ=.1 GeV	.080	3.2
Q.C.D. Λ=.2 GeV	.076	3.6
Q.C.D. Λ=.3 GeV	.070	4.4
Q.C.D. Λ=.4 GeV	.063	5.5

From this comparison we can conclude that Q.C.D. perturbation theory is not sufficient for computing the properties of the ground state of the $(t\bar{t})$ system for m_t=45 GeV/c^2.

In view of the considerations above, I will use only Richardson's potential for all results for the top system in the balance of these lectures.

As the first application of quarkonium physics to the top system, consider the spectrum (ignoring relativistic corrections) of $(t\bar{t})$ states below the threshold for Zweig allowed decays into a pair of mesons with open top. This threshold can be estimated by comparison to the bottom system[23] If M_T is the mass of the ground state pseudoscalar $(t\bar{u})$ open top meson, and M_B is the mass of the corresponding pseudoscalar in the $(b\bar{u})$ system (M_B=5.273 GeV), then

$$M_T - m_t = M_B - m_b + 3/4\ (M_{B*} - M_B)(1-m_b/m_t) \qquad (2.6)$$

where $M_{B*}-M_B$ ~50 MeV/c and m_b=4.8 GeV. Thus

$$M_T = m_t + .43\ \text{GeV} \quad . \qquad (2.7)$$

The spectrum of $(t\bar{t})$ states for m_t=45 GeV is shown in Figure 10. Let me mention some of the impressive features of this

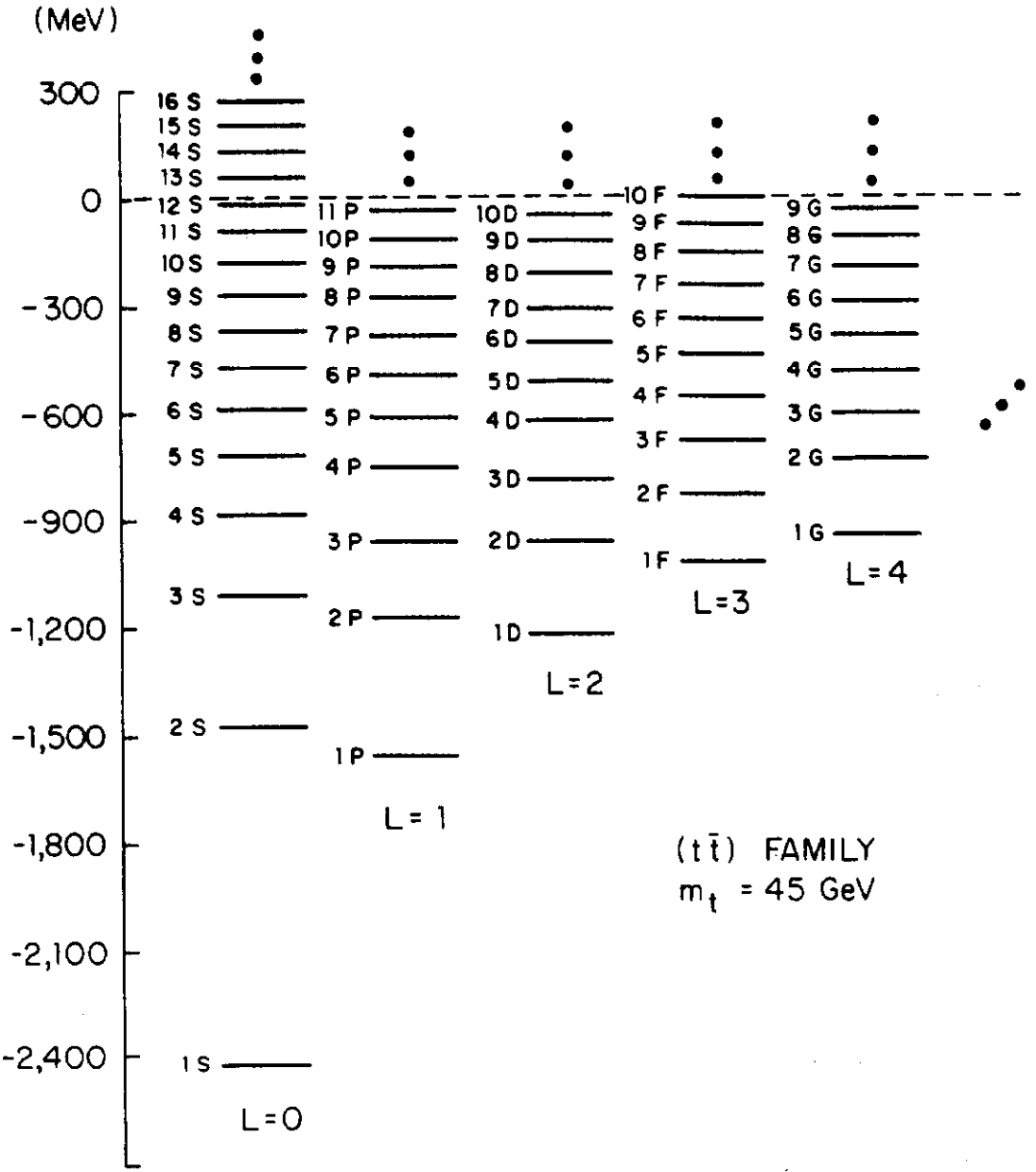

Figure 10: The spectrum of $(t\bar{t})$ states for $m_t = 45$ GeV using Richardson's potential. The vertical scale is the binding energy (MeV) of the $(t\bar{t})$ state relative to the threshold for Zweig allowed decays (dashed line). The states are displayed by orbital angular momentum L. All states below threshold with $L \leq 4$ are shown explicitly. The maximum L for which at least one state is below threshold is $L_{max} = 17$.

spectrum:

(1) The ground state 1S ($t\bar{t}$) state is 2.415 GeV below threshold.

(2) There are 12 S states below threshold and hence relatively narrow.

(3) The spacing between successive S states decreases from 946 MeV for the 2S-1S splitting to less than 100 MeV for states near threshold. In particular, the 12S-11S splitting is only 80 MeV.

(4) The maximum orbital angular momentum for which the associated ground state is below threshold is L=17.

(5) Remembering that for each S state shown there are two degenerate states (S=0) J=0 and (S=1) J=1 and for every other L value there are four degenerate states (S=0) J=L and (S=1) J=L+1, L, L-1; there are a total of 424 ($t\bar{t}$) states below threshold.

(6) Since the states near threshold are quite densely packed, they are ideal for application of semiclassical (WKBJ) methods.[20]

Some of the other useful properties of the low-lying states are:

(a) The Binding Energies

$t\bar{t}$ State	Binding Energy $[2M_T - m(t\bar{t})]$ (MeV)	
1S	2,415	946
2S	1,469	359
3S	1,110	
1P	1,566	
1D	1,235	

(b) For the 1S ($t\bar{t}$) state

$$\langle R^2\rangle^{1/2} = 0.058 \text{ fm}$$
$$\langle v^2/c^2\rangle^{1/2} = 0.14 \quad .$$

(c) The electronic widths of the n^3S_1 states are given by

$$\Gamma_0^{e^+e^-}(n) \equiv \frac{16\pi\, e_Q^2\alpha^2}{M_n^2(t\bar{t})}\,|\psi_n(0)|^2 \tag{2.8}$$

We will postpone the discussion of electroweak corrections until the next section; however the perturbative Q.C.D. corrections can be included to lowest order in α_s to give

$$\Gamma^{e^+e^-}(n) = \Gamma_0^{e^+e^-}(n)\left(1 - \frac{16\alpha_s(2m_t)}{3\pi} + O(\alpha_s^2)\right) \tag{2.9}$$

For the 1S state

$$\Gamma_0^{e^+e^-}(1) = 8.5 \text{ keV} \tag{2.10}$$

with a strong correction factor ~.8. For the excited states

$$\Gamma_2/\Gamma_1 = .27$$
$$\Gamma_3/\Gamma_1 = .11 \qquad \text{and } \Gamma_{12}/\Gamma_1 = .05 \tag{2.11}$$
$$\Gamma_4/\Gamma_1 = .075$$

Finally consider the effects of including the leading relativistic corrections -- the spin-dependent splittings -- which give the fine and hyperfine structure of the spectrum.

For a discussion of the theory of spin-dependent forces see

Ref. 1. The general result for the spin-dependent potential[24] is:

$$V_{\substack{\text{Spin}\\ \text{Dependent}}}(R) = \left(\frac{\vec{S}_1\cdot\vec{L}}{2m_1^2} + \frac{\vec{S}_2\cdot\vec{L}}{2m_2^2}\right)\frac{1}{R}\left(\frac{d\mathcal{E}}{dR} + \frac{2dV_1}{dR}\right)$$

$$+ \frac{(\vec{S}_1+\vec{S}_2)\cdot\vec{L}}{m_1 m_2}\,\frac{1}{R}\,\frac{dV_2}{dR} \qquad (2.12)$$

$$+ \frac{2}{3m_1m_2}\,\vec{S}_1\cdot\vec{S}_2 V_4$$

$$+ \frac{1}{m_1m_2}\left[(\vec{S}_1\cdot\hat{R})(\vec{S}_2\cdot\hat{R}) - \frac{1}{3}\,\vec{S}_1\cdot\vec{S}_2\right] V_3$$

where $(m_1,\vec{S}_1)$ and $(m_2,\vec{S}_2)$ refer to the mass and spin of the quark and antiquark respectively. $\mathcal{E}(R)$ is the nonrelativistic potential in Q.C.D. The potentials $V_i(R)$ $(i=1,\ldots,4)$ are the spin-dependent potentials which can be determined numerically in principle by Lattice Monte Carlo methods. So far this has not been done, and thus we must rely to some extent on phenomenological assumptions to obtain these potentials.

In the last year an important new relation between these V's has been shown by D. Gromes[25] to hold in Q.C.D. He shows that

$$V_1(R) = V_2(R) - \mathcal{E}(R) \qquad (2.13)$$

This relation makes the simplest phenomenological assumption[24] about the nature of Electric Confinement (i.e., V_1, V_2, V_3, and V_4 all short range and hence perturbatively calculable) inconsistent with Q.C.D. Both V_1 and V_2 cannot be simultaneously short range

since by definition $\mathcal{E}(R)$ contains the long range confining part of the potential. The most straightforward remedy to this situation is to assume that only those potentials which arise from correlations involving the gauge magnetic field and also depend on the position of both the quark and antiquark are short range.[25] With this revised assumption as to the consequences of Electric Confinement, V_2, V_3, and V_4 would be assumed to be short range. This has the feature that long range contributions still arise only in the Spin-Orbit terms, however the form of their appearance is modified. The Spin-Orbit terms in Eq. (2.13) can now be reexpressed as:

$$V_{\substack{\text{Spin}\\\text{Orbit}}}(R) = \left(\frac{\vec{S}_1 \cdot \vec{L}}{2m_1^2} + \frac{\vec{S}_2 \cdot \vec{L}}{2m_2^2} \right) \frac{1}{R} \left(- \frac{d\mathcal{E}(R)}{dR} + 2V_2(R) \right) \qquad (2.14)$$

$$+ \frac{(\vec{S}_1 + \vec{S}_2) \cdot \vec{L}}{m_1 m_2} \frac{1}{R} V_2(R) \quad .$$

This form of Electric Confinement Model is now in agreement with the so-called Scalar Confinement Models[26] for the spin-dependent forces. Hence there now seems to be a common model of the spin-dependent forces. The Scalar Confinement Models have long been known to be phenomenologically favored in the $(c\bar{c})$ system.[27] This development provides a very satisfying resolution to the previous problems modeling the spin-dependent forces.[28]

Let us turn from general discussion to specific application to the $(t\bar{t})$ system. It will suffice for our purposes to make rough estimates of the fine and hyperfine splittings in the $(t\bar{t})$ system.

The hyperfine mass splitting between the spin triplet and singlet S states

$$\Delta(nS) = m(n^3S_1) - m(n^1S_0) \tag{2.15}$$

is determined by the V_4 term in Eq. (2.13). It is expected that this interaction is short range and hence calculable in perturbation theory. The result in perturbation theory is given by[29]

$$\Delta(nS) = \frac{8}{3}\frac{|\psi_n(0)|^2}{M^2(nS)}\,4\pi\,\frac{4}{3}\,\alpha_{\overline{MS}}(M)\left[1+\frac{\alpha_{\overline{MS}}\xi}{\pi}+\ldots\right] \tag{2.16}$$

where

$$\xi = 0.562 + 0.375\left[\frac{\left\langle \ln Q^2/M^2\right\rangle_{nS}}{|\psi_n(0)|^2}\right] \tag{2.17}$$

using $\Lambda_{\overline{MS}}$=.17 GeV which fits the ψ-η_c splitting and gives Υ-η_b splitting ≈30 MeV/c we can determine the splitting for the $(t\bar{t})$ system. For m=45 GeV, $\alpha_{\overline{MS}}(m_{t\bar{t}})$≈.12 and the α^2_{MS} term in Eq. (2.16) is only a 10% correction. Ignoring this small correction we have

$$\Delta(nS) = \frac{8/9\ \alpha_{\overline{MS}}}{e_Q^2\ \alpha_{EM}^2}\,\Gamma_0^{e^+e^-}(n) \quad ; \tag{2.18}$$

using Eq. (2.10) and (2.11)

$$\begin{aligned}\Delta(1S) &\simeq 40\ \text{MeV}\\ \Delta(2S) &\simeq 11\ \text{MeV}\end{aligned} \tag{2.19}$$

and

$$\Delta(nS) = \Gamma^{e^+e^-}_{(n)} / \Gamma^{e^+e^-}_{(1)} \Delta(1S) \qquad n>2 \quad .$$

Thus the possibility of observing the singlet states through these M1 transitions is remote. The ground state $^1S_0(t\bar{t})$ state (η_t) can also be accessed via hadronic or hindered M1 transitions from the excited S states (e.g. the $2^3S_1(t\bar{t})$ state). I postpone the discussion of this possibility until the next lecture. The spin-orbit and tensor structure of Eq. (2.13) contributes to the triplet P state splittings. These splittings have been measured in the $(c\bar{c})$[27] and $(b\bar{b})$[30] systems. In general we may write

$$\begin{aligned} m(^3P_2) &= M_0 + a - 2/5\ c \\ m(^3P_1) &= M_0 - a + 2c \\ m(^3P_0) &= M_0 - 2a - 4c \end{aligned} \tag{2.20}$$

where M_0 is the mass of the Center of Gravity of the triplet P state system, a is the spin-orbit contribution

$$a = \frac{1}{2m_t^2} \left\{ -\left\langle \frac{1}{R} \frac{d\varepsilon}{dR} \right\rangle_P + 2\left\langle \frac{1}{R} \frac{dV_2}{dR} \right\rangle_P \right\} \tag{2.21}$$

and c is the tensor contribution

$$c = \frac{1}{3m_t^2} \left\langle V_3 \right\rangle_P \quad . \tag{2.22}$$

Here $\langle\ \rangle_P$ denotes the expectation in the nonrelativistic P state. In order to obtain a rough estimate of the size of these splittings in the $(t\bar{t})$ system, we can approximate ε by the Cornell Model

Coulomb plus linear form. While V_2 and V_3 are given in perturbation theory and are of the form:

$$V_3 \simeq \frac{1}{R}\frac{dV_2}{dR} \simeq \frac{4}{3}\frac{\alpha_s(R)}{R^3} \tag{2.23}$$

The long range part of the splitting comes from the term

$$\langle K/R \rangle_{1P} \simeq .5\ \text{GeV}^3 \tag{2.24}$$

while the short range part comes from

$$\left\langle \frac{4}{3}\frac{\alpha_s(R)}{R^3} \right\rangle_{1P} \simeq \alpha_s(\text{eff}) \times 20\ \text{GeV}^3 \tag{2.25}$$

with a typical value of $\alpha_s(\text{eff}) \simeq .2$. Hence the perturbative contribution clearly dominates; very little can be learned about the nonperturbative contributions from the study of the fine structure of the low-lying P states. Even more disappointingly, for the triplet 1P state

$$\begin{aligned} a &= 2\ \text{MeV} \\ c &= .7\ \text{MeV} \end{aligned} \tag{2.26}$$

making the splittings (Eq. 2.20) unobservably small.

III. PRODUCTION AND DECAY

Observation of the rich spectrum of $(t\bar{t})$ states shown in Figure 10 depends on the production properties for the $J^{PC}=1^{--}$ state in e^+e^- collisions. Below threshold for Zweig allowed hadronic decays some of the $(t\bar{t})$ states with different J^{PC} may be accessed through hadronic and photonic transitions from the excited triplet S states. The decay rates of the n^3S_1 states are needed to determine the relevant branching fractions of these transitions and thus to assess the feasibility of observing these other states. Above threshold the principal decay of the $n^3S_1(t\bar{t})$ states is into pairs of open top mesons.

I now turn to this discussion of production and decay both below and above threshold for open top decay.

Toponium Decays

The spin triplet $(t\bar{t})$ ground state ($^3S_1$) has only direct decays via $(t\bar{t})$ annihilation or weak decay of one of the top quarks. The excited states can decay both directly and by hadronic and photonic transitions to lower mass $(t\bar{t})$ states.

First consider the decays of the lowest $^3S_1$ state. Since the top quark masses is so large we can no longer ignore the full electroweak interactions. It will be assumed in this section that $|M_V-M_Z|>>\Gamma_Z$ (the width of the Z^0) so that mixing between any $(t\bar{t})$ state (V) and the Z^0 can be treated perturbatively. The situation in the special case that $|M_V-M_Z|\leq\Gamma_Z$ is discussed in the final

lecture. Then denoting $u_i = (u,c,t,\nu_e,\nu_\mu,\nu_\tau)$ for $i=1,\ldots,6$ and $d_i = (d,s,b,e,\mu,\tau)$ for $i=1,\ldots,6$

$$\begin{aligned}\mathcal{L}_I = \sum_i \Big\{ & e\, A_\mu \Big[Q_{u_i} \bar{f}_{u_i} \gamma^\mu f_{u_i} + Q_{d_i} \bar{f}_{d_i} \gamma^\mu f_{d_i} \Big] \\ & + \frac{g_W}{\sqrt{2}} \Big[W^+_\mu \bar{f}_{u_i} \gamma^\mu \frac{(1-\gamma_5)}{2} f_{d_i} + \text{h.c.} \Big] \\ & + \frac{g_W}{2\cos\theta_W} Z^0_\mu \Big[\bar{f}_{u_i L} \gamma^\mu \frac{(1-\gamma_5)}{2} f_{u_i} + \bar{f}_{d_i L} \gamma^\mu \frac{(1-\gamma_5)}{2} f_{d_i} \\ & + \bar{f}_{u_i R} \gamma^\mu \frac{(1+\gamma_5)}{2} f_{u_i} + \bar{f}_{d_i R} \gamma^\mu \frac{(1+\gamma_5)}{2} f_{d_i} \Big] \Big\}\end{aligned} \tag{3.1}$$

where g_W is the weak coupling, θ_W is the Weinberg angle, $M_Z \simeq 93$ GeV, and $M_W \simeq 82$ GeV. The couplings $L_f \equiv (\tau_3)_f - 2Q_f x_W$ and $R_f \equiv -2Q_f x_W$ where $(\tau_3)_f = +1$ for $f=u_i$ and -1 for $f=d_i$, Q_f is the fermion's charge, and $x_W = \sin^2\theta_W$.

The decays of the $1^3S_1(t\bar{t})$ state (V) into charged leptons proceed through the virtual photon and Z^0 as shown in Figure 11a. The ratio of the total leptonic decays to the contribution from virtual photons is given by[31,32]

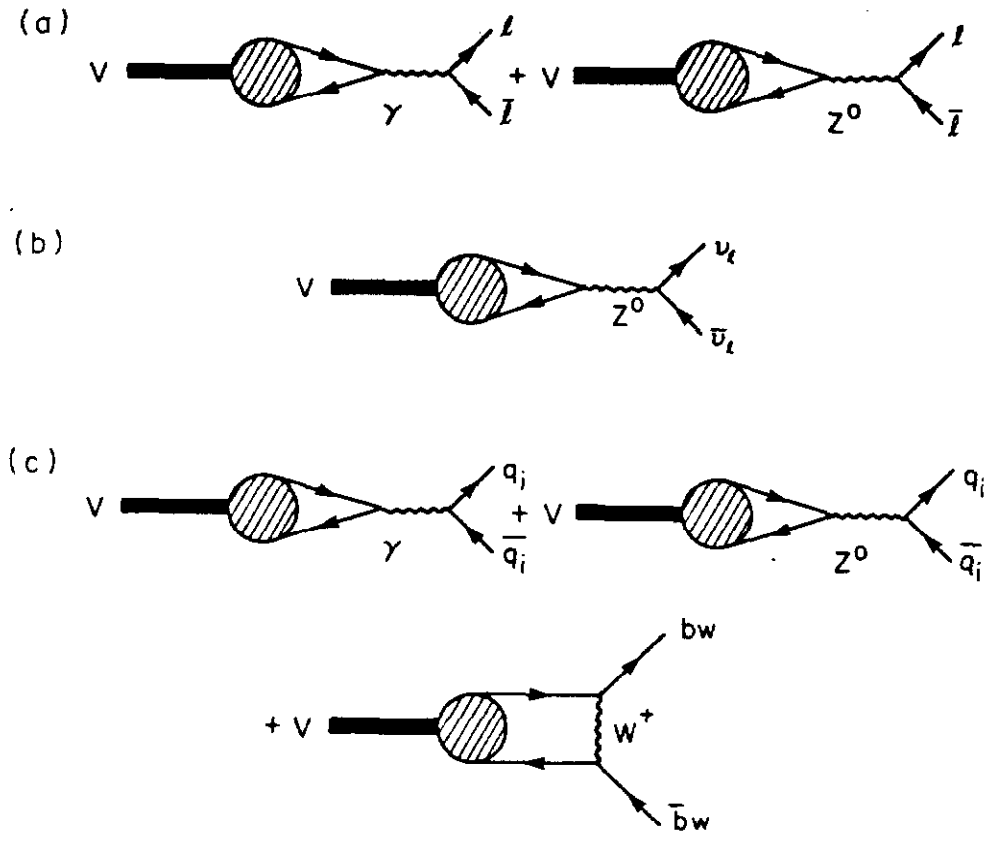

Figure 11: Processes contributing to V decays into: (a) charged lepton pairs, (b) neutrino pairs, and (c) quark pairs. b_w denotes the bottom quark weak eigenstate.

$$R = \frac{\Gamma(V\to\ell^+\ell^-)}{\Gamma(V\to"\gamma"\to\ell^+\ell^-)} = 1 +$$

$$\frac{1}{Q_t Q_\ell}\,\frac{(L_t+R_t)(L_\ell+R_\ell)}{8x_W(1-x_W)}\left[\frac{m_V^2/m_Z^2(1-m_V^2/m_Z^2)}{(1-m_V^2/m_Z^2)^2+\Gamma_Z^2/m_Z^2}\right] \qquad (3.2)$$

$$+\,\frac{1}{Q_t^2 Q_\ell^2}\,\frac{(L_t+R_t)^2(L_\ell^2+R_\ell^2)}{64x_W^2(1-x_W)^2}\left[\frac{m_V^4/m_Z^4}{(1-m_V^2/m_Z^2)^2+\Gamma_Z^2/m_Z^2}\right]$$

where $L_\ell=-1+2x_W$, $R_\ell=2x_W$, and $L_t+R_t=-1+{}^8/_3\,x_W$. Therefore

$$\Gamma(V\to\ell^+\ell^-) = R\,\frac{16\pi\alpha^2 Q_t^2 Q_\ell^2}{M_V^2}\,|\psi_V(0)|^2\left(1-\frac{16\alpha_s(M_V)}{3\pi}+\ldots\right). \qquad (3.3)$$

For decays into neutrinos only the virtual Z^0 can contribute. The process is shown in Figure 11b. The decay rate is

$$\Gamma(V\to\nu_\ell\bar{\nu}_\ell) = \frac{16\pi\alpha^2}{M_V^2}\,|\psi_V^2(0)|\left(1-\frac{16\alpha_s(M_V)}{3\pi}+\ldots\right)$$

$$\times\left\{\frac{(1-{}^8/_3\,x_W)^2\left[4x_W^2+(1-2x_W)^2\right]}{64x_W^2(1-x_W)^2}\right\} \qquad (3.4)$$

$$\left[\frac{m_V^4/m_Z^4}{\left[(1-m_V^2/m_Z^2)^2+\Gamma_Z^2/m_Z^2\right]}\right]$$

Annihilation to final states involving $q_i\bar{q}_i$ via γ or Z^0 in the

s channel or $W^{\pm}$ in the t channel is shown in Figure 11c. For the W exchange contribution the momentum transfer is $t \approx -M_V^2/4$. If we ignore the masses of all final state quarks and approximate the $W^{\pm}$ exchange by a point interaction ($-t \ll M_W^2$), then[33]

$$\frac{\Gamma(V \to q_i \bar{q}_i)}{\Gamma(V \to "\gamma" \to \ell^+ \ell^-)} = 3\, Q_q^2\, R\{L_\ell, R_\ell, Q_\ell \to L_q, R_q, Q_q\}$$

$$- \frac{|U_{tq}|^2 Q_q}{12 x_W Q_t} \frac{M_V^2}{M_W^2 + 1/4\, M_V^2} \left(1 + \frac{M_V^2}{8 M_W^2} \right)$$

$$- \frac{1}{3} \frac{|U_{tq}|^2}{Q_t^2} \frac{L_q(L_t + R_t)}{32 x_W^2 (1 - x_W)^2} \frac{M_V^2}{M_W^1 + 1/4\, M_V^2} \qquad (3.5)$$

$$\left\{ \left[\frac{m_V^2/m_Z^2 (1 - m_V^2/m_Z^2)}{(1 - m_V^2/m_Z^2)^2 + \Gamma_Z^2/m_Z^2} \right] \left(1 + \frac{M_V^2}{8 M_W^2} \right) \right\}$$

$$+ \frac{1}{9} \frac{|U_{tq}|^4}{32 x_W^2 Q_t^2} \frac{M_V^4}{(M_W^2 + 1/4\, M_V^2)^2} \left(1 + \frac{M_V^2}{8 M_W^2} \right)^2$$

Where R was defined in Eq. (3.1) with $L_q = (\tau_3)_q - 2Q_q x_W$ and $R_q = -2Q_q x_W$. The K-M matrix U couples the top quark to a linear combination of the bottom, strange, and down quark (denoted b_w) which is predominately the bottom quark.

Finally the weak decay of the top quark is shown in Figure 12.

The rate for the weak top quark decay in the limit $m_t < m_W$ is given by[34]

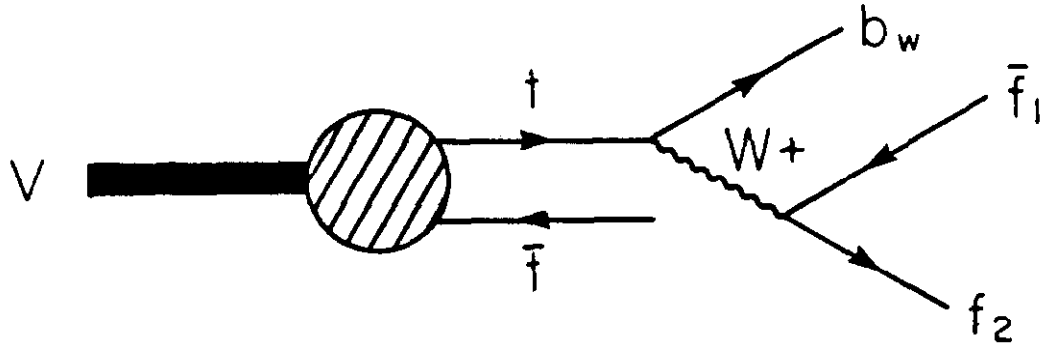

Figure 12: V decays associated with top quark weak decays. f_1 and f_2 are any pair of quarks or leptons which couple to the W^+ as shown.

$$\Gamma(V\to d_i f_1 \bar{f}_2) = \left\{ \begin{array}{ll} 1 & f = \text{lepton} \\ 3 & f = \text{quark} \end{array} \right\} \frac{G_F^2 m_t^5}{192\pi^3}$$

$$\left[|U_{f_2 f_1}|^2 \, |U_{t d_i}|^2 \int_0^1 dx \, \frac{2(1-3x^2+2x^3)}{\left(1-\frac{x m_t^2}{M_W^2}\right)^2 + \Gamma_W^2/m_W^2} \right] \tag{3.6}$$

where d_i = b, s, or d and $(f_1,\bar{f}_2) = (u,\bar{d})$, $(c,\bar{s})$, (ν_e,e^-), (ν_μ,μ^-) or (ν_τ,τ^-). Of course for $m_t > m_W + m_b$ the real W^+ decays will dominate; then

$$\Gamma(V\to b+W^+) = \frac{G_F m_t^3}{8\pi\sqrt{2}} |U_{tb}|^2 \left(1 - \frac{m_W^2}{m_t^2}\right)^2 \left(1 + \frac{2m_W^2}{m_t^2}\right) \tag{3.7}$$

The other decay modes of the $^3S_1$ $(t\bar{t})$ states are the usual gluon decays shown in Figure 13. We have[35]

$$\frac{\Gamma(V\to 3g)}{\Gamma(V\to "\gamma"\to \ell^+\ell^-)} = \frac{5}{18}\left(\frac{\pi^2-9}{\pi}\right) \frac{\alpha_s^3(M_V)}{\alpha^2} \tag{3.8}$$

and

$$\frac{\Gamma(V\to 2g\gamma)}{\Gamma(V\to 3g)} = \frac{16}{5}\,\frac{\alpha}{\alpha_s} \quad . \tag{3.9}$$

Some more exotic decays are discussed in the next lecture.

Combining the various decays we can compute the branching ratios for virtual electroweak decays (Eqs. (3.2), (3.3), (3.4) and (3.5)), weak top decays (Eq. (3.6)), three gluon decays (Eq. (3.8)), and photon plus two gluon decay (Eq. (3.9)). The results as a

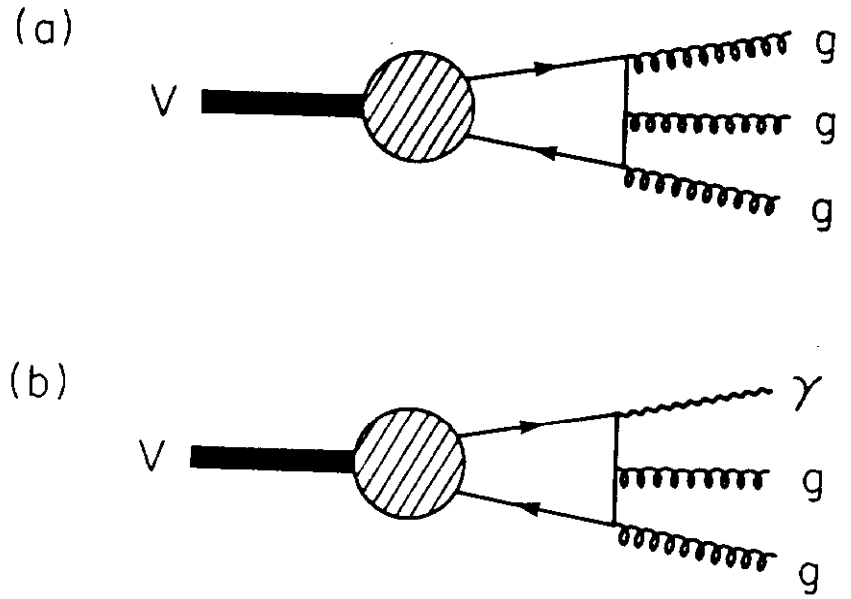

Figure 13: Processes contributing to V decay rate associated with: (a) strong (i.e. three gluon) decays and (b) single photon and two gluon decays.

function of the top quark mass are shown in Figure 14. The two most prominent features of Figure 14 are:

(1) For toponium masses near the Z^0 mass the decays of the ground $^3S_1$ state are completely dominated by the virtual Z^0 decays; and

(2) For $m_t \geq m_{Z^0}/2$ the weak decay of the top quark via a virtual W begin to become dominant. Hence the standard strong interaction decays which dominated ψ and Υ decays become relatively unimportant for $m_t \gtrsim 40$ GeV/c^2, the electroweak interactions become dominant.

The theory for hadronic transitions has been discussed recently in Ref. 1. The basic calculational approach is to make a multipole expansion for gluon radiation similar to the usual multipole expansion for photon radiation. The main difficulty is how to model the gluon to light hadron transitions. Kuang and Yan[36] have used a vibrating string model for the total rates for the transitions $n^3S_1 \to m^3S_1 + 2\pi$ and $n^3S_1 \to m^1S_0 + \eta$. The results for the 2π transitions are shown in Figure 15. To estimate the total hadronic transition rates they simply ignore hadronization of the produced gluons.

The photon transitions can be calculated by standard methods. The largest photonic transitions are E1 transitions. For example, the transitions $n^3S_1 \to m^3P_J + \gamma$ proceed at the rate:

$$\Gamma_{E1}(n^3S_1 \to m^3P_J + \gamma) = \frac{16\alpha}{243} k^3 (2J+1) \left| \int_0^\infty dR \; U_{nS}(R) R \; U_{mP}(R) \right|^2 \qquad (3.10)$$

where k is the photon momentum and U_{nS} and U_{mP} are the radial

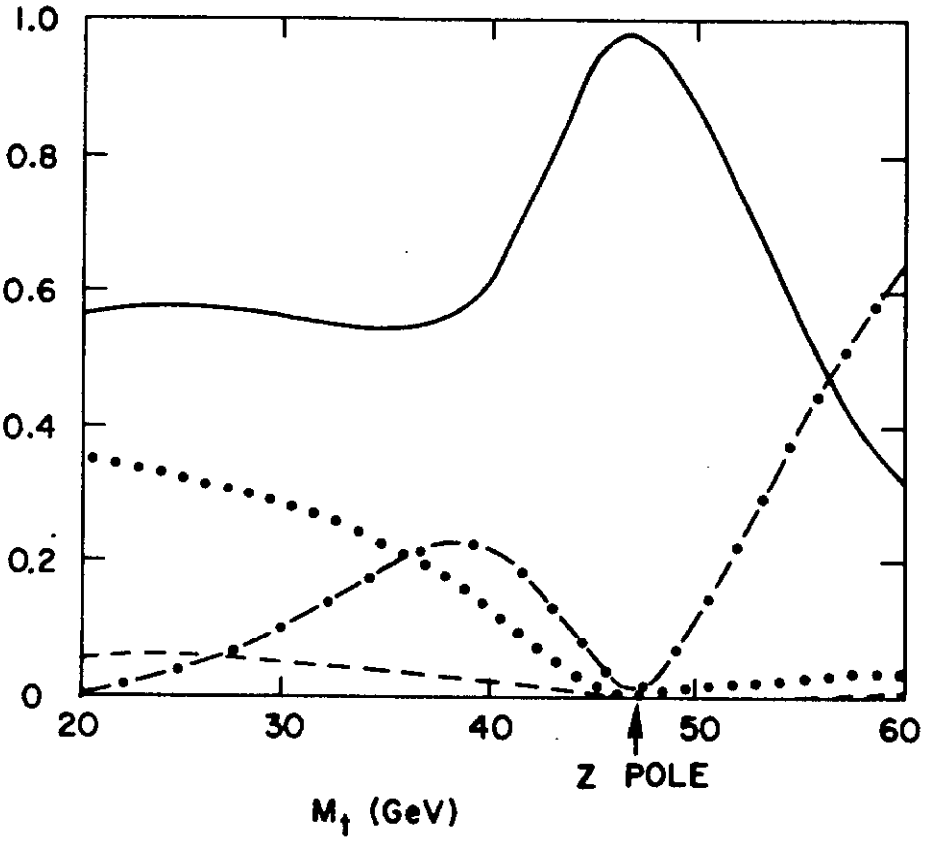

Figure 14: The decay branching ratios for the 1^3S_1 ($t\bar{t}$) state (V) as a function of the top quark mass. The solid curve is the contribution of the virtual electroweak decays; the dotted curve the three gluon decays; the dot-dashed curve the $W^{\pm}$ weak decays of the top quark; and the dashed curve the two gluon-photon decays.

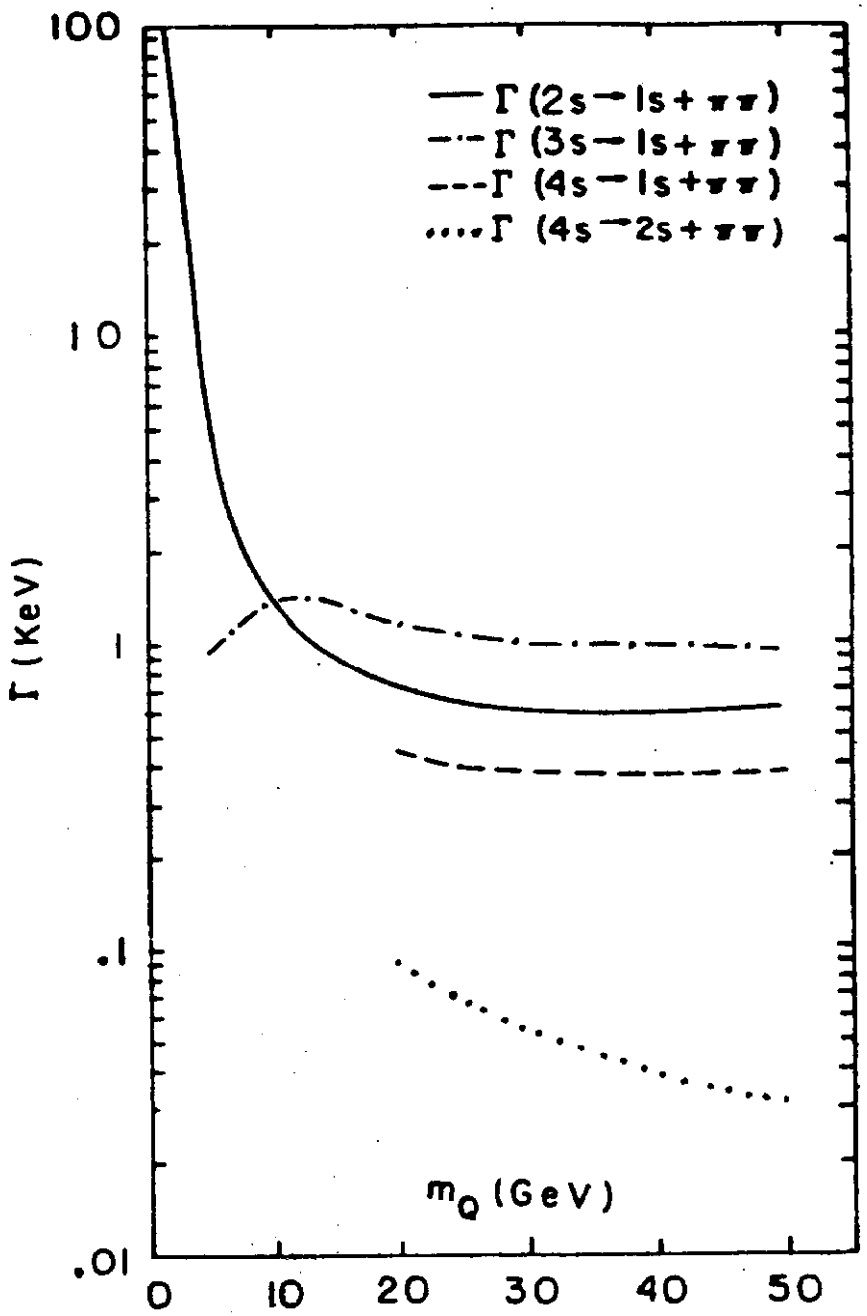

Figure 15: The hadronic transitions $n^3S_1 \rightarrow m^3S_1$ plus two pions. The solid curve is the (n=2, m=1) transition; the dot-dashed curve is the (n=2, m=1) transition; the dashed curve is the (n=4, m=1) transition; and the dotted curve is the (n=4, m=2) transitions. This figure is taken from Ref. 36.

wavefunctions of the nS and mP state, respectively. For m_t in the range 20-60 GeV/c^2 the photonic transitions for low-lying excited $^3S_1(t\bar{t})$ states scale approximately as $4(m_b/m_t)^{2/3}$ from the corresponding state in the $(b\bar{b})$ system.

The resulting partial decay widths for direct decays, hadronic transitions, and photonic transitions for a representative excited $^3S_1$ state are shown in Figure 16. Again for top quark masses 40 GeV/c^2 direct decays dominate. This makes the $(t\bar{t})$ states with J^{PC} other than 1^{--} essentially inaccessible via transitions from excited $^3S_1$ states.

Production of Toponium and Open Top

The production of a narrow resonance (V) in e^+e^- collisions has an integrated area

$$\int dW\ \Delta R(W) = \frac{9\pi}{2\alpha^2}\ \Gamma(V\to e^+e^-) \tag{3.11}$$

where ΔR is the enhancement in R at center of mass energy W due to the resonance

$$\Delta R(W) \equiv \frac{\sigma(e^+e^-\to V)}{\sigma(e^+e^-\to \text{"}\gamma\text{"}\to\mu^+\mu^-)} \quad . \tag{3.12}$$

By convention the cross section is compared to the $\mu^+\mu^-$ cross section (through the virtual photon only) to define R. The peak R is determined in terms of the mean center of mass energy spread of the collider $(\Delta W)_{rms}$ by

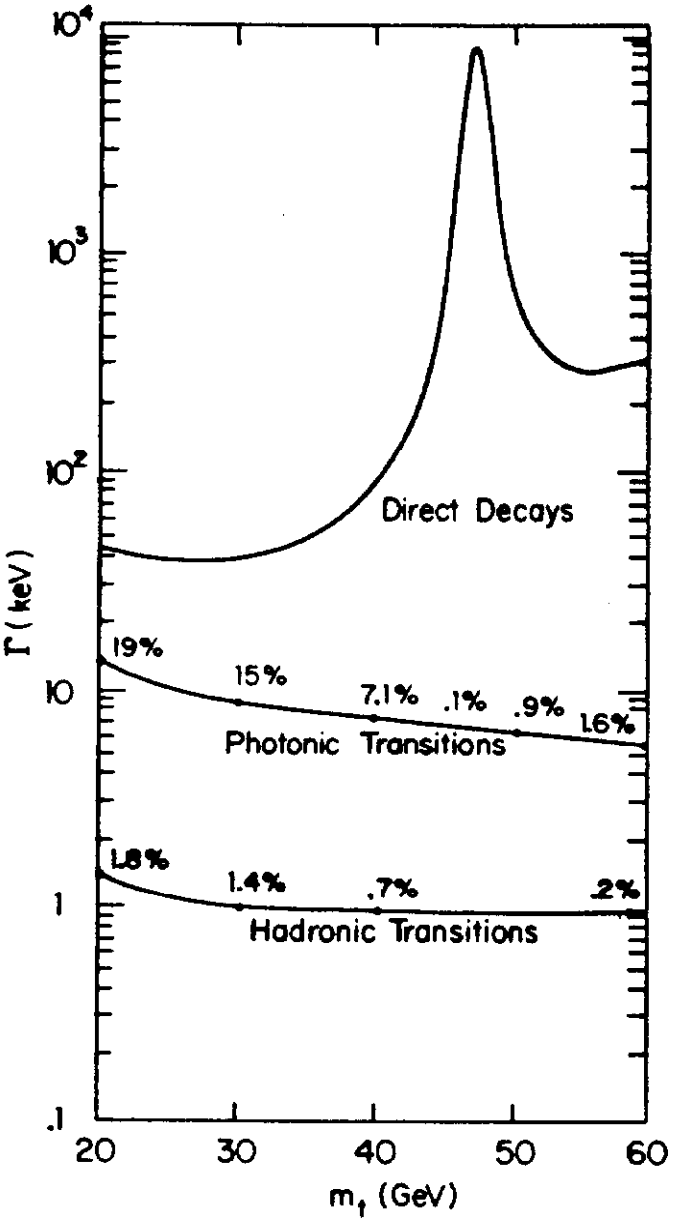

Figure 16: The partial widths of the 3^3S_1 ($t\bar{t}$) state as a function of top quark mass m_t (in GeV). The direct decays and photonic and hadronic transitions are shown. For the transitions the branching ratios (in percents) are shown at various values of m_t.

$$R_{peak} = \frac{9\pi}{2\alpha^2} \frac{\Gamma(V\to e^+e^-)}{(\Delta W)_{rms}\sqrt{2\pi}} \quad . \tag{3.13}$$

For the Stanford Linear Collider (SLC) the expected resolution is

$$(\Delta W)_{rms} = 100 \left(\frac{E_{beam}}{50\ GeV} \right)^2 MeV \tag{3.14a}$$

While for LEP the nominal $(\Delta W)_{rms}$ is

$$(\Delta W)_{rms} = 40 \left(\frac{E_{beam}}{50\ GeV} \right) MeV \tag{3.14b}$$

We can apply these general results to the toponium ($t\bar{t}$) resonances below threshold for Zweig allowed decays. For the 1^3S_1 state $\Gamma(e^+e^-)\approx 8$ keV so at SLC with an average luminosity

$$\mathcal{L} = 2\times 10^{31} \left[\frac{E_{beam}}{50\ GeV} \right]^2 cm^{-2} sec^{-1} \tag{3.15}$$

$$= 2000 nb^{-1}/day \left[\frac{E_{beam}}{50\ GeV} \right]^2$$

we have [37]

	$e^+e^- \to$ all		$e^+e^- \to \mu^+\mu^-$	
$M(t\bar{t})$ GeV	R_{Total} (Background)	ΔR (Signal)	$R_{\mu\mu}$ (Background)	$\Delta R_{\mu\mu}$ (Signal)
50	7	34	1.03	3.4
60	9	22	1.08	2.1
70	14	18	1.3	1.3
80	43	18	2.2	.85
90	830	110	28.	3.8
93	5710	600	191.	24.
96	1020	134	35.	4.5
100	248	38	9.	1.2

The ratio of R_{peak} to $R_{background}$ (for LEP) as a function of center of mass energy is shown in Figure 17. These results do not include radiative corrections which would result in the following modifications:[37] $(\Delta W)_{observed} = 2.355(\Delta W)_{rms}$, $R_Z(\text{corrected}) \simeq {}^2/_3\, R_Z(\text{bare})$, and $\Delta R_V(\text{corrected}) \simeq {}^1/_2\, \Delta R_V(\text{bare})$. The reader should also be cautioned that when a $(t\bar{t})$ resonance lies within the width of the Z peak, then can be important interference effects which are ignored here. (This is discussed in the next lecture.)

Since a $\Delta R=1$ corresponds to approximately two events per day with the luminosity given in Eq. (3.15), it should be relatively easy to observe the lowest $^3S_1(t\bar{t})$ state with any mass in the range accessible to LEPI and SLC. However the situation for the excited states is more complicated. The electronic widths decrease rapidly for the excited n^3S_1 state. Using Eq. (2.11) and the above table of $\Delta R(1S)$, we see that ΔR is already $\lesssim 2$ for the 3^3S_1 resonance except near the Z^0 pole. Hence only a few of the low-lying $^3S_1$ resonances in the $(t\bar{t})$ system will be easily observable for toponium masses away from the Z^0 pole. Even in the vicinity of the Z^0 pole, because

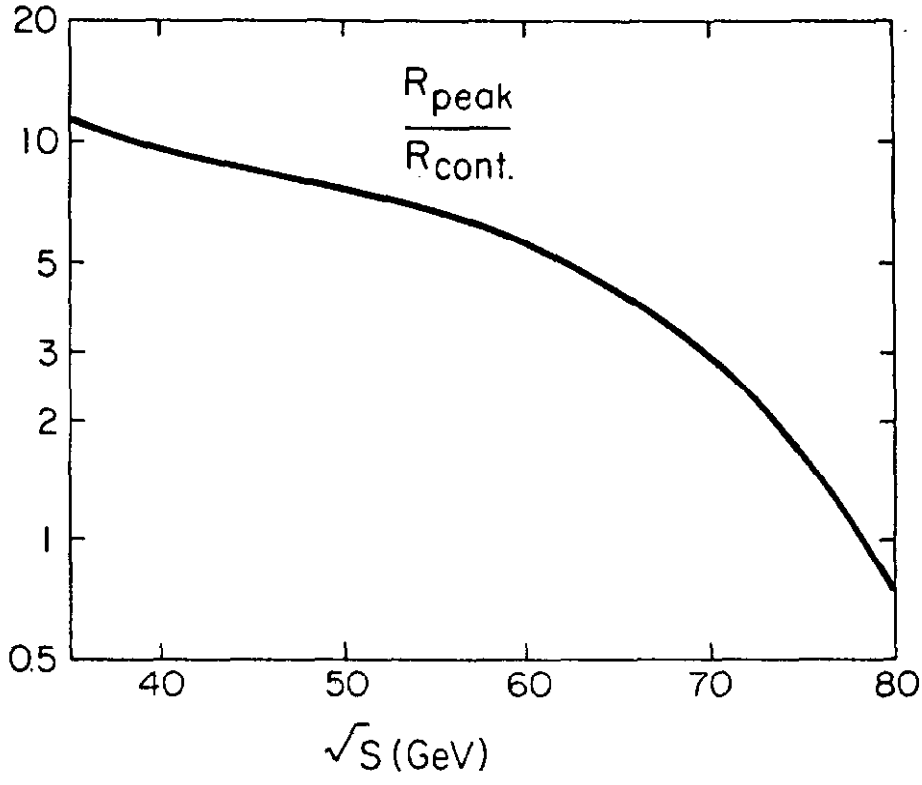

Figure 17: The ratio of R at the peak of the 1^3S_1 ($t\bar{t}$) resonance to the background (continuum) R is shown as a function of resonance mass (GeV) for the energy resolution expected at LEP. (Figure is taken from Ref. 37.)

the spacing between successive levels decreases with increasing n (as shown in Figure 10), resolving the separate resonance near threshold will be problematic. For example, the $(12^3S_1-11^3S_1)$ splitting is only 80 MeV. Resolution better than the nominal 100 MeV resolution at SLC will be required. However 50 MeV resolution should be sufficient to resolve this structure.

As the threshold for Zweig allowed decays is crossed the $(t\bar{t})$ resonances can decay into open top meson pairs; hence the natural widths of these states will be significantly enhanced. The corresponding threshold region in the $(c\bar{c})$ and $(b\bar{b})$ systems is shown in Figures 18a and 18b. As in these other systems, the ΔR above threshold in the $(t\bar{t})$ systems would be expected to have structure for slightly less than 1 GeV above threshold and the widths of resonances just above threshold to be 30-50 MeV. Since the energy resolution of the colliders in this energy range is at least as large as these widths any structure in the peaks associated with the opening of individual decay channels will be washed out. If the machine resolution is worse than ~80 MeV the resonances in the threshold region will overlap leaving a relatively smooth ΔR as threshold is crossed. Even if 40 MeV resolution is achieved, the natural widths of states above threshold will not be much larger than resolution; hence the distinction between narrow resonances below threshold and wide resonances above will be blurred. Thus we will not be able to use the shape of ΔR to infer when the open top production threshold has been crossed.[38]

Finally we consider the decay products of the $(t\bar{t})$ resonances

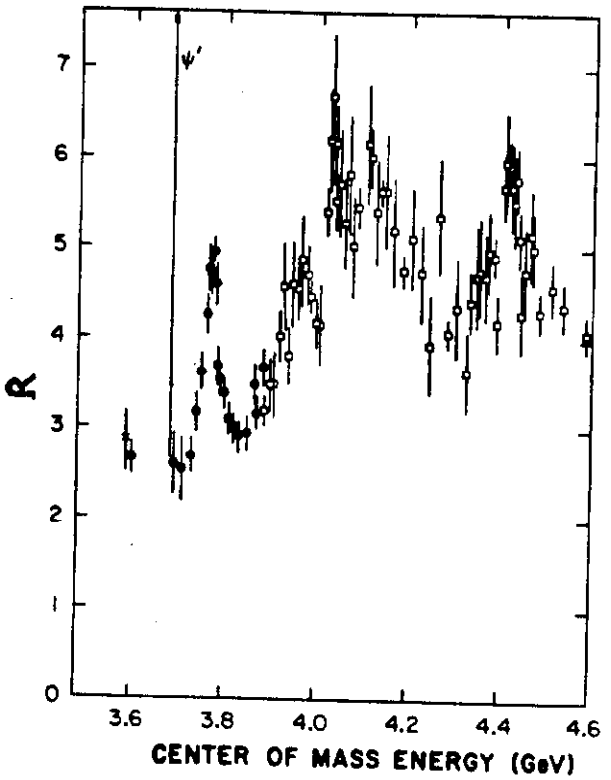

Figure 18(a): The threshold behaviour of R in the $(c\bar{c})$ system. From Ref. 38.

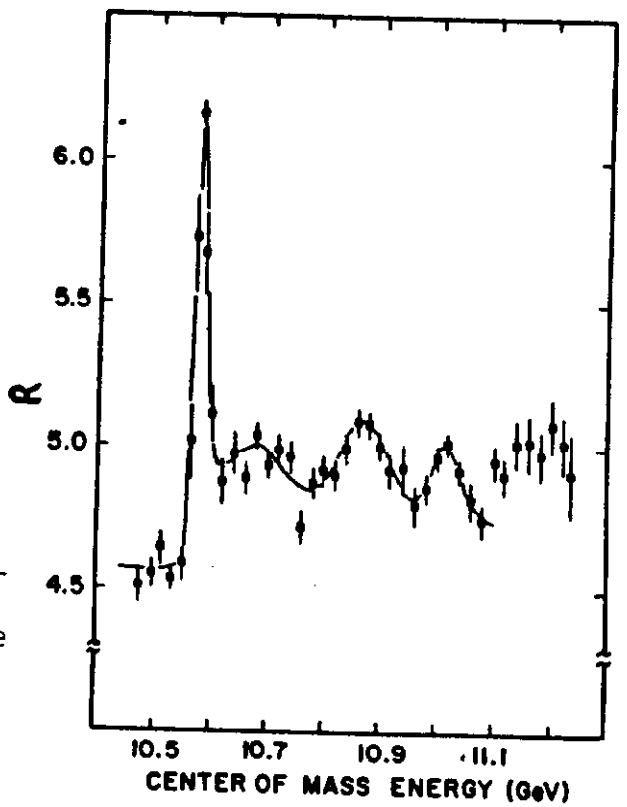

Figure 18(b): The threshold behaviour of R in the $(b\bar{b})$ system. From Ref. 39.

above threshold -- the open top mesons. There are some novel features of the low-lying open top mesons.

The open top system is an ideal heavy (Q) - light (q) quark system. In non-relativistic quantum mechanics the energy of a two body system ($\mathcal{E}^0$) depends on the particle masses through the reduced mass

$$\mu = \frac{m_Q m_q}{m_Q+m_q} = m_q - \frac{m_q^2}{m_Q} + \ldots \tag{3.16}$$

i.e., μ becomes independent of m_Q as $m_Q \to \infty$. The corrections ($\mathcal{E}^1$) due to finite m_Q are partially given by the second term in μ which represents recoil corrections and the spin-spin ($\mathcal{E}^0_{SS}$) and tensor ($\mathcal{E}^0_T$) hyperfine interaction. The spin-orbit interaction has a piece ($\mathcal{E}^0_{LS}$) which survives even in $m_Q \to \infty$ limit as well as $1/m_Q$ correction term ($\mathcal{E}^1_{LS}$). Hence the mass of a heavy-light system can be expanded in powers of $1/m_Q$ to give:[6,23]

$$\begin{aligned} M(n;\ell;J^{PC};m_Q^{-1}) = m_Q + \left[\mathcal{E}^0_0(n,\ell) + \vec{L}\cdot\vec{S}_q\mathcal{E}^0_{LS}(n,\ell)\right] \\ + \frac{m_q^2}{m_Q}\left\{\vec{S}_Q\cdot\vec{S}_q\mathcal{E}^0_{SS}(n,\ell) + T_{12}\mathcal{E}^0_T(n,\ell) + \right. \\ \left. + (\vec{S}_Q+\vec{S}_q)\cdot\vec{L}\,\mathcal{E}^1_{LS}(n,\ell) + \mathcal{E}^1(n,\ell)\right\} + O\left(\frac{m_q^3}{m_Q^2}\right) \end{aligned} \tag{3.17}$$

where $T_{12} \equiv \langle nJ\ell j|(\vec{S}_Q\cdot\hat{R})(\vec{S}_q\cdot\hat{R}) - \frac{1}{3}\vec{S}_q\cdot\vec{S}_q|nJ\ell j\rangle$. Note that the terms independent of m_Q depend only on $\vec{L}^2=\ell(\ell+1)$, $\vec{S}_q^2=3/4$, and $\vec{j}=\vec{L}+\vec{S}_q$.

Unfortunately, for reduced masses $\mu \lesssim 1$ GeV potential model

calculations of the various energies ($\mathcal{E}$'s) are unreliably. Hence for the $(t\bar{u})$, $(t\bar{d})$, and $(t\bar{s})$ meson systems one is forced to use data from some other heavy-light system to determine the $\mathcal{E}$'s. The only data presently available is for the ground (1S) states: $(D^*,D)^{0,+}$ for the $(c\bar{u})$ and $(c\bar{d})$ systems, and $(B^*,B)^{-,0}$ for the $(b\bar{u})$ and $(b\bar{d})$ systems.

For the ground states of $(Q\bar{u})$ and $(Q\bar{d})$ systems Eq. (3.17) simplifies to

$$M = m_Q + \mathcal{E}^0 + \frac{1}{m_Q}\left(\mu^2\mathcal{E}^1 + \vec{S}_Q\cdot\vec{S}_q\mu^2\mathcal{E}^0_{SS}\right) \quad . \tag{3.18}$$

So the hyperfine splitting is

$$M\left[{}^3S_1(Q\bar{q})\right] - M\left[{}^1S_0(Q\bar{q})\right] = \frac{1}{m_Q}\left\{\mu^2\mathcal{E}^0_{SS}(\mu^2)\right\} \quad . \tag{3.19}$$

Thus

$$M(B^*) - M(B) = \frac{m_c}{m_b}\left[m(D^*)-m(D)\right] \simeq 3.5\left[145\ \text{MeV}\right] \simeq 50\ \text{MeV} \tag{3.20}$$

in agreement with recent measurement.[41] For the open top system we denote

$$\begin{aligned} T^{*0} &\equiv {}^3S_1(t\bar{u}) & T^{*+} &\equiv {}^3S_1(t\bar{d}) \\ T^0 &\equiv {}^1S_0(t\bar{u}) & T^+ &\equiv {}^1S_0(t\bar{d}) \end{aligned} \tag{3.21}$$

Using Eq. (3.18) we conclude

$$\left[m(T^*) - m(T)\right] = \frac{m_b}{m_t}\left[m(B^*) - m(B)\right] \quad . \tag{3.22}$$

For m_t=45 GeV and using Eq. (3.20) and (3.22) we expect

$$m(T^*) - m(T) \simeq 6 \text{ MeV} \quad . \tag{3.23}$$

This mass splitting is much smaller than expected width of $(t\bar{t})$ resonances above thresholds. Hence mass differences do not significantly alter the statistical ratios for relative production of $T\bar{T}$, $T^*\bar{T}+T\bar{T}^*$, and $T^*\bar{T}^*$ final states (1:4:7). The dominate decay mode for $(t\bar{t})$ resonances near threshold should be $T^*\bar{T}^*$.[42]

The mass difference between vector and pseudoscalar open top mesons is so small that it is comparable to the T^+-T^0 mass splitting. To accurately estimate this last mass splitting, remember two sources of this T^+-T^0 mass splitting must be included. First, the current algebra up-down quark mass difference. This was estimated by Lane and Weinberg[43]; m_d-m_u=4.84. Second, electroweak gauge interactions. In this second class we include:

(1) t channel γ and Z^0 exchanges with the general form: $e_Q e_q(A_0+A_1/m_Q)$,

(2) electroweak contributions to the quark masses themselves with the general form $e_Q^2 B_1+e_q^2 B_2$, and

(3) interactions involving additional quark loops.

To a good approximation we may ignore interaction terms with additional quark loops and hyperfine terms (i.e., A_1/m_Q); then the mass splitting will be identical to the $(c\bar{d})$ and $(c\bar{u})$ systems. So[44]

$$m(T^+) - m(T^0) = m(D^+) - m(D^0) = 4.7 \pm .3 \text{ MeV} \tag{3.24}$$

and since only the A_1/m_t term is sensitive to the difference between T* and T we have to the same good approximation

$$m(T^{*+}) - m(T^{*0}) = m(T^+) - m(T^0) \quad . \tag{3.25}$$

The spectrum of ground state open top mesons is shown in Figure 19.

The only allowed transition of T* to T is via a M1 photonic transition. The rate is

$$\Gamma(T^* \to \gamma T) = \frac{1}{3} \alpha\, k^3 \left(\frac{e_t}{m_t} + \frac{e_q}{m_q}\right)^2 \tag{3.26}$$

where $m_q \sim 300$ MeV and $k \simeq 6$ MeV. Thus

$$\Gamma(T^* \to \gamma T) \simeq e_q^2 (5.8 \text{ eV}) \tag{3.27}$$

while the weak decays via virtual W^+ proceed at the rate

$$\Gamma_{weak}(T^*) = \Gamma_{weak}(T) \simeq \frac{9}{192\pi^3} G_F^2 m_t^5 \tag{3.28}$$

which for $m_t = 45$ GeV/c^2 gives $\Gamma_{weak} \sim 30$ keV. Hence the transition $T^* \to \gamma + T$ is completely unobservable.[31]

The excitation spectrum for the open top meson systems ($t\bar{c}$) and ($t\bar{b}$) can be calculated using nonrelativistic potentials and spin-dependent corrections as in the ($c\bar{c}$) and ($b\bar{b}$) systems. The results for the nonrelativistic spectrum are shown in Figure 20. For the ($t\bar{u}$), ($t\bar{d}$) and ($t\bar{s}$) systems all we can say with confidence is that the excitation spectrum is independent of m_t up to corrections of order (300 MeV/m_t).

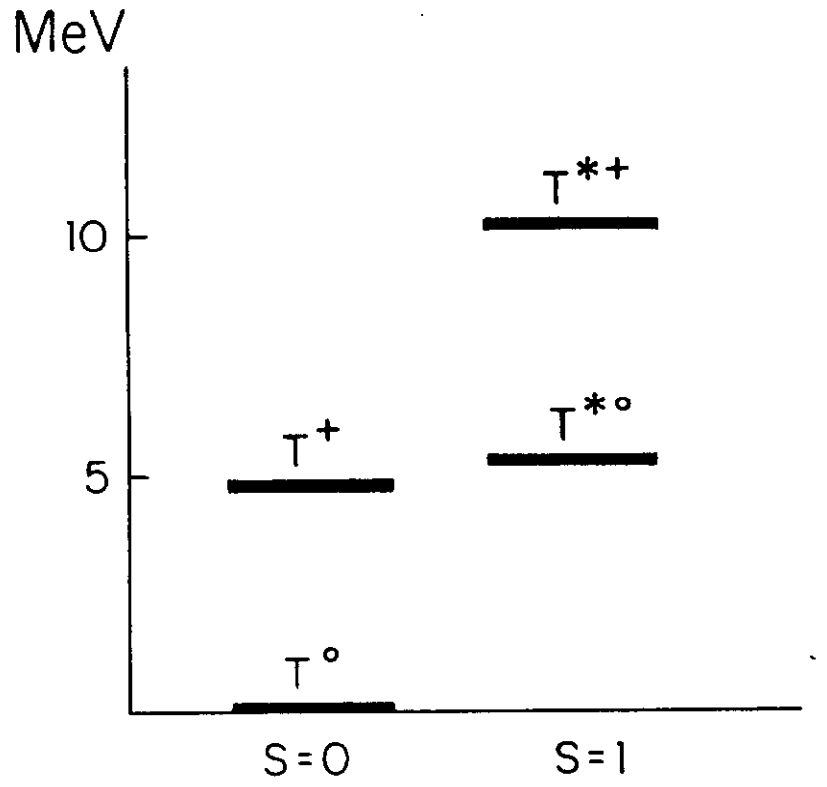

Figure 19: The excitation spectrum for ground state spin zero (pseudoscalar) and spin 1 (vector) open top mesons. T^0, T^{*0} are the $(t\bar{u})$ states while T^+, T^{*+} are the corresponding $(t\bar{d})$ states.

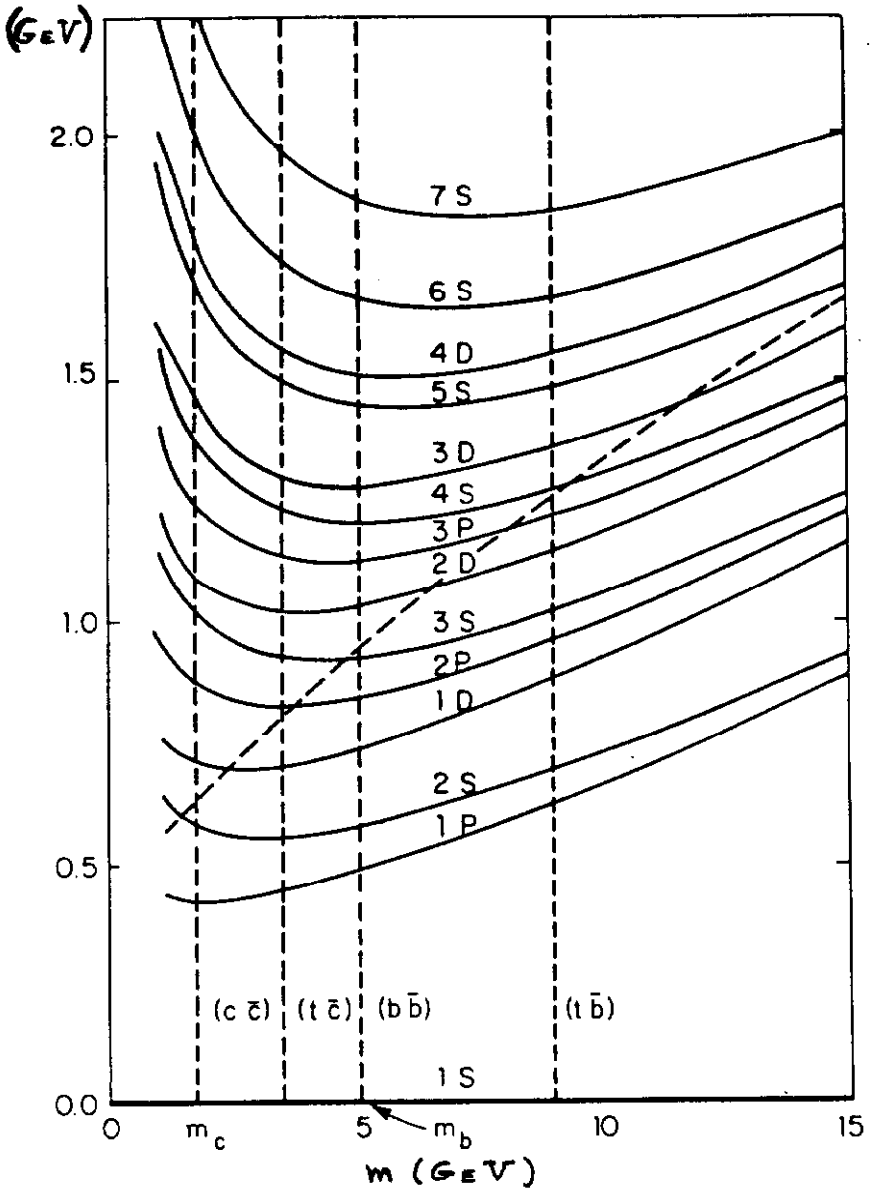

Figure 20: The excitation spectrum for heavy-heavy systems is shown as a function of the reduced mass in GeV of the system. The excitation energy (in GeV) is computed using the Cornell potential of Ref. 6. The slanted dashed line is the threshold for Zweig allowed decays while the vertical dashed lines are the reduced mass at the $(c\bar{c})$, $(t\bar{c})$, $(b\bar{b})$, and $(t\bar{b})$ systems left to right.

IV. SOME EXOTIC POSSIBILITIES

Here I will discuss three nonstandard possibilities for the physics of the toponium system.

Decays Involving Higgs-Like Scalars

The scalar sector of the electroweak interactions is still completely unknown experimentally. In the minimal (W-S) model there is only one doublet of elementary scalar fields and the only physical state after EW symmetry breakdown is a neutral Higgs scalar H^0. In non-minimal models or extended technicolor models there can be more than one doublet.[45] There the set of physical spin zero fields include two neutral (H^0,$H^{0'}$) and a pair of charged (H^+,H^-) fields. If these scalars are sufficiently light the ground state $^3S_1$ ($t\bar{t}$) will have decay modes involving these scalars.

For the standard neutral Higgs scalar (H^0) the 1^3S_1 state (denoted below by V) may decay into H^0 plus photon. This Wilczek process[46] is shown in Fig. 21a. For $m(H^0) < m(V)$

$$\Gamma(V\rightarrow\gamma+H^0) = \frac{G_F\, m_t^2}{\sqrt{2}\,\alpha\,\pi}\left[1 - \frac{m_H^2}{m_V^2}\right]\Gamma_{"\gamma"}(V\rightarrow\mu^+\mu^-) \qquad (4.1)$$

where $\Gamma_{"\gamma"}$ is the decay rate through only the virtual proton. The branching ratio for this decay is shown in Fig. 22 for M(V) = 75 GeV. Since ΔR_{peak} is 18 and $= 10^{31}cm^{-2}sec^{-1}$ at SLC for $\sqrt{s}$ = 75 GeV there are 35 events/day of V production. For $m(H^0)$ = 60 GeV the branching ratio shown in Fig. 22 is approximately 1% and hence there are ~100 events/year for the $H^0 + \gamma$ decay.

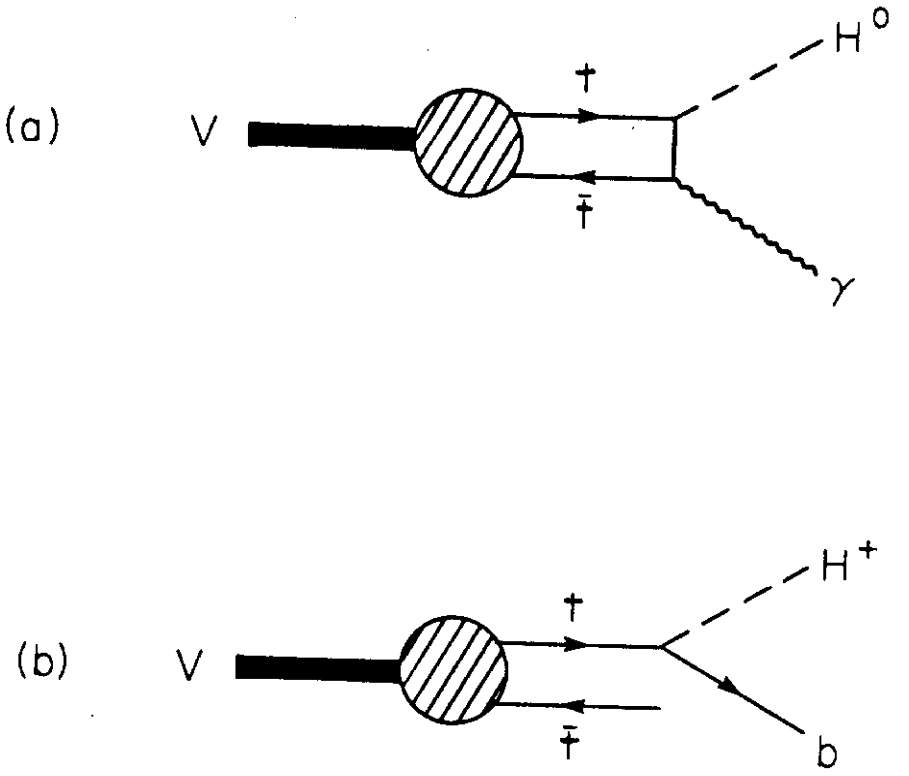

Figure 21: The decays of 1^3S_1 ($t\bar{t}$) state (denoted V here) involving electroweak scalar decay products. The decay to neutral Higgs scalar and photon is shown in (a) and the semi-weak decay of the top quark to possible charged Higgs and bottom quark is shown in (b).

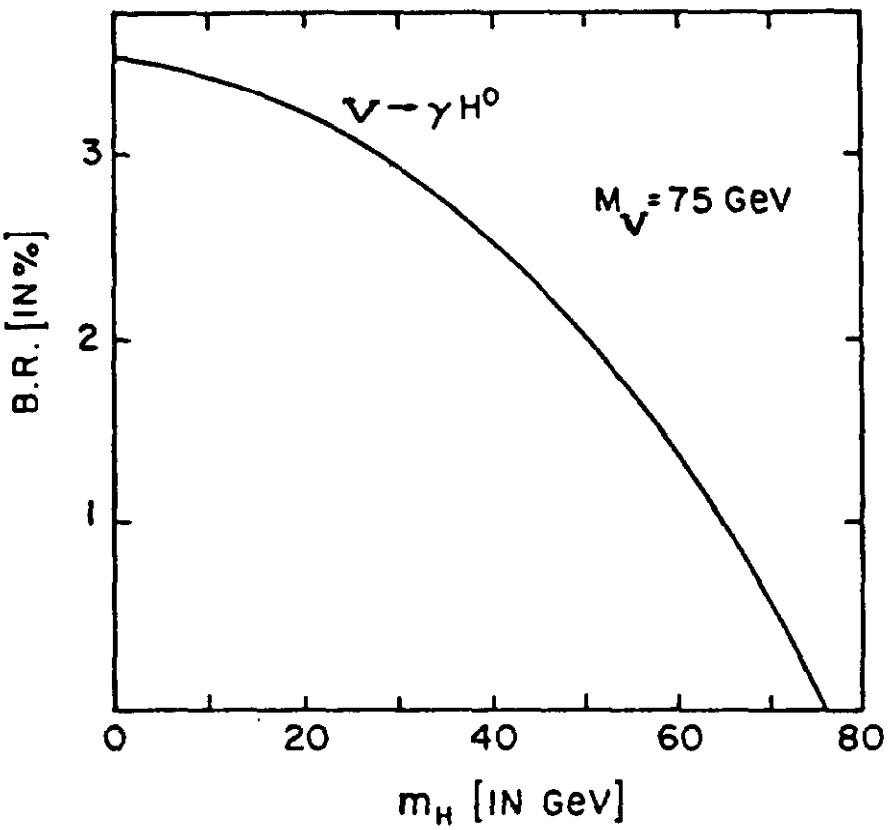

Figure 22: The branching ratio of $1^3S_1(t\bar{t})$ (denoted V) to $\gamma+H^0$ as a function of m_{H^0}. Here M_V=75 GeV. Figure taken from Ref. 37.

For $m(V) > 75$ GeV the direct decay of V through the virtual Z^0 s channel pole and top quark decays dominate (see Fig. 14). This makes the decay mode $H^0 + \gamma$ unobservably small even with no kinematic suppression due to $m(H^0)$.

In non minimal models there are also charged spinless particles ($H^{\pm}$). The coupling of H^+ to $t\bar{b}$ is

$$U_{tb}\, m_t \sqrt{G_F}\, (\sqrt{2})^{1/2} \tag{4.2}$$

and the decay process for the toponium resonance V is shown in Fig. 21b. If the decay $t \to H^+ + b$ is kinematically allowed it will completely dominate all other decays of any $(t\bar{t})$ system as shown in Fig. 23. Seeing conventional top quark decays into electrons in the UA1 experiment at the $Sp\bar{p}S$ collider rules out any H^+ which couples to mass with $m(H^+) \lesssim m_t - 5$ GeV.

Direct P State Production

Because the Z^0 has an axial vector coupling as well as a vector coupling the $J^{PC} = 1^{++}$ states of the $(t\bar{t})$ system can also be directly produced in e^+e^- collisions (see Fig. 24). However nonrelativistically the wave function at the origin vanished except for S states, hence the production will be suppressed relative to S state vector production. The strongest production will be for the smallest orbital angular momentum -- the P states. This possibility has been studied in detail by J. Kuhn and S. Ono.[47] The production

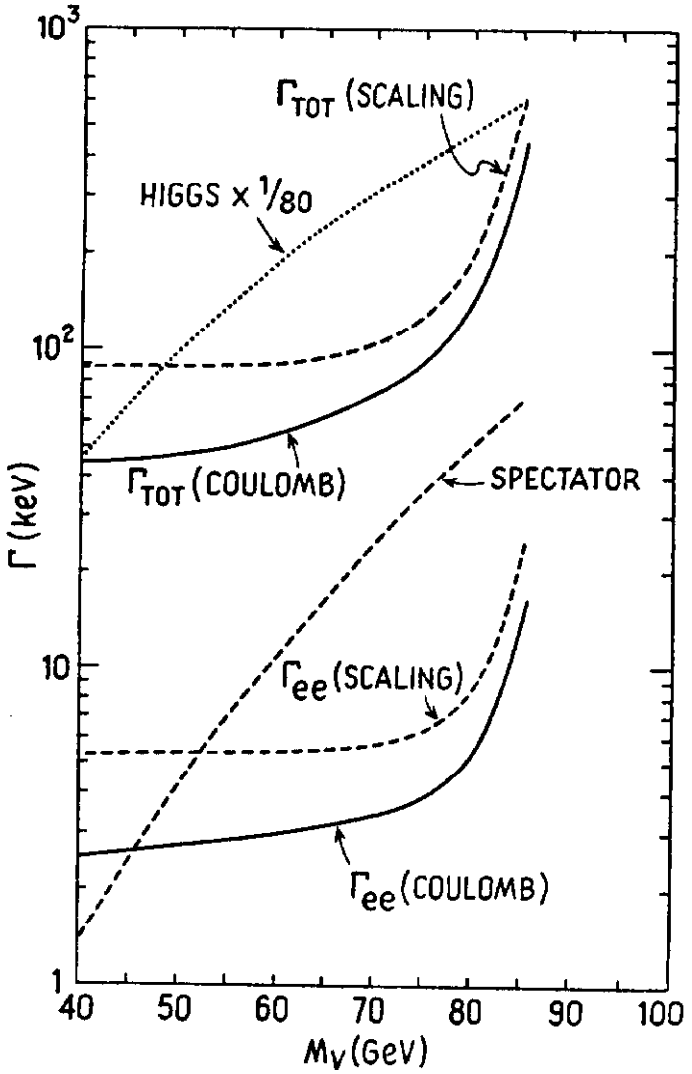

Figure 23: The dotted line represents 1/80 of the width for the decay of the 1^3s_1 toponium state of mass M_V into a charged Higgs scalar of mass 8 GeV. The total and electronic decay widths are shown for comparison. The potential model dependency of the usual decays is modeled by using two extreme cases. The solid (dashed) lines are based on Coulombic wave functions (scalar laws) discussed in Ref. 33. The contribution from weak decays at the top quark is also shown explicitly (spectator line). The figure is taken from Ref. 33).

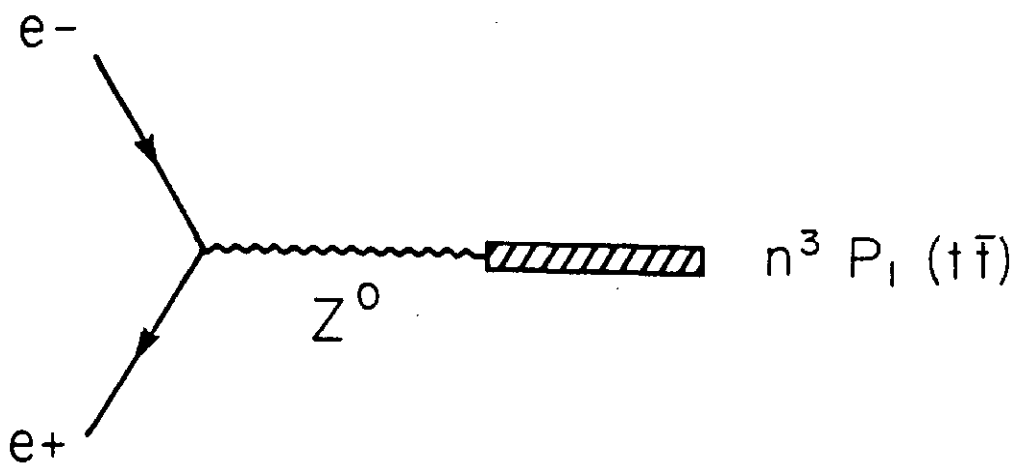

Figure 24: Direct production in e^+e^- collision of the n^3P_1 $(t\bar{t})$ states through the axial vector coupling of the virtual Z^0.

rate for $e^+e^- \to {}^3P_1(t\bar{t})$ state through the virtual Z^0 is given using Eq. (3.1) from the partial decay rate

$$\Gamma\left({}^3P_1(t\bar{t}) \to e^+e^-\right) = \frac{3\left(L_e^2+R_e^2\right)}{2\pi^2}\left(G_F M_Z^2\right)^2 \frac{|R_p'(0)|^2}{\left(M_p^2-M_Z^2\right)^2 + \Gamma_Z^2 M_Z^2} \quad (4.3)$$

where $|R_p'(0)|$ is the derivative of the radial wavefunction at the origin for the particular P state. For M_t = 45 GeV:

State	$\lvert R_p'(0)\rvert$ $(\mathrm{fm}^{-5/2})$
1P	2375
2P	1985

For the $1P(t\bar{t})$ state at $M_p \simeq M_Z$

$$\Gamma\left(1^3P_1 \to e^+e^-\right) = 22 \text{ keV} \quad . \quad (4.4)$$

At SLC this corresponds to a ΔR_{peak} = 23 and therefore production of the $1^3P_1(t\bar{t})$ state at a rate of approximately 50 events/day. Of course for top masses much below $m_Z/2$ the Z^0 contribution is small and consequently direct P state production is unobservable.

Toponium-Z^0 Mixing

As the mass of any $n^3S_1(t\bar{t})$ state (V) becomes sufficiently close to the Z^0 mass the mixing between these two states may become significant and lead to large interference effects. The coupling of V to Z^0 is depicted in Fig. 25. This coupling is of order e and has the dimensions of mass squared. Defining the coupling to be $e\, g_{VZ}$, there will be no significant mixing for

$$\left| e\, g_{VZ} \frac{1}{\left(M_V^2 - M_Z^2\right) - i\Gamma_{Z_0} M_{Z_0}} \right| \ll 1 \quad . \tag{4.5}$$

The width of the V state has been ignored in Eq. (4.5) since it is only 20 keV without mixing to the Z^0. Vector meson dominance determines the photon coupling to V[48]

$$e\, g_{V\gamma} = 2\sqrt{3}\, Q_t e \sqrt{M_V}\, \psi_V(0) \tag{4.6}$$

while for the Z^0 coupling

$$\frac{g_{VZ}}{g_{V\gamma}} = \frac{1}{Q_t} \frac{(L_t + R_t)}{2\sin 2\theta_w} = 0.375 \quad . \tag{4.7}$$

For $m_t = 45$ GeV the 1^3S_1 state has $|\psi_V(0)|^2 \approx 64\ \text{GeV}^3$ and thus

$$e\, g_{VZ} \approx 20\ \text{GeV}^2 \quad . \tag{4.8}$$

Now near the Z^0 pole ($M_V \approx M_Z$) Eq. (4.5) becomes

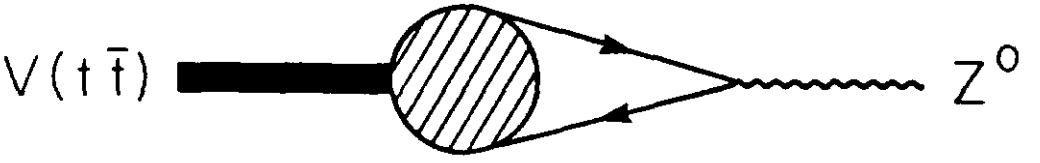

Figure 25: Lowest order mixing between the toponium state (denoted V) and the Z^0.

$$\frac{eg_{VZ}}{2M_Z}\left|\frac{1}{(M_V-M_Z-i\Gamma_{Z/2})}\right| \simeq 0.11\ \text{GeV}\left|\frac{1}{M_V-M_Z-i\Gamma_{Z/2}}\right| . \qquad (4.9)$$

Thus the mixing is very small unless $|M_V - M_Z| \lesssim \Gamma_Z$.

Recently the interference between toponium and the Z^0 has been studied in detail by P. Franzini and F. Gilman[49] and also J.H. Kühn, and P.M. Zerwas.[50] Here I will discuss only the simple model of $V - Z^0$ mixing proposed by F.M. Renard[51]. I have however modified the discussion to be consistent with these new studies. The reader is referred to Refs. [49] and [50] for more complete discussions.

Consider the mixing of Z^0 with single resonance V of the toponium system which is below the threshold for decays into open top. Starting with the unmixed states denoted $|V_0\rangle$ and $|Z_0\rangle$ and the complex mass matrix

$$\mathcal{M} = \begin{bmatrix} M_{Z_0} - i\Gamma_{Z_0}/2 & m_{VZ} \\ m_{VZ} & M_{V^0} - i\Gamma_{V^0}/2 \end{bmatrix} \qquad (4.10)$$

we can determine the physical eigenstates.

The real part of the mixing term is simply

$$\text{Re}(m_{VZ}) = \frac{eg_{VZ}}{2M_V} = \frac{e(1-8/3\ \sin^2\theta_W)}{2\sin 2\theta_W}\ \sqrt{3}\ \frac{|\psi_V(0)|}{\sqrt{M_V}} \qquad (4.11)$$

while the Im $(m_{VZ}) \simeq 0$ below threshold. Above threshold the imaginary part arising from open top meson pair intermediate states can be significant.

The physical eigenstates $|V\rangle$ and $|Z\rangle$ can be expressed in terms of the bare states using a complex angle θ.

$$\begin{aligned} |Z\rangle &= \cos\theta\ |Z_0\rangle + \sin\theta\ |V_0\rangle \\ |V\rangle &= -\sin\theta\ |Z_0\rangle + \cos\theta\ |V_0\rangle \end{aligned} \tag{4.12}$$

The orthogonality of the physical states $|V\rangle$ and $|Z\rangle$ requires[52]

$$\langle V|\mathcal{M}|Z\rangle = 0 \tag{4.13}$$

which implies

$$\tan 2\theta = \frac{2\, m_{VZ}}{\Delta M_0 - i\Delta\Gamma_0/2} \equiv A \tag{4.14}$$

where $\Delta M_0 \equiv M_Z^0 - M_V^0$ and $\Delta\Gamma_0 \equiv \Gamma_Z^0 - \Gamma_V^0$.

With a little trigonometry we may reexpress Eq. (4.14) as

$$\sin\theta = \left[\frac{(\sqrt{A^2+1} - 1)}{2\sqrt{A^2+1}} \right]^{1/2} \underset{A \text{ small}}{\sim} A/2 \ . \tag{4.15}$$

Now the shifts of masses and modifications of widths are determined by

$$\begin{aligned} \langle Z|\mathcal{M}|Z\rangle &\equiv M_Z - i\Gamma_{Z/2} \\ &= \left(M_Z^0 - i\Gamma_{Z/2}^0\right) + \sin^2\theta\ \left(-\Delta M_0 + i/2\ \Delta\Gamma_0\right) \\ &\quad + \sin 2\theta\ m_{VZ} \ . \end{aligned} \tag{4.16}$$

Hence defining $\delta M_Z \equiv M_Z - M_Z^0$ and $\delta\Gamma_Z = \Gamma_Z - \Gamma_Z^0$ we have

$$\delta M_Z - i/2\ \delta\Gamma_Z = m_{VZ}\ \left[\sqrt{1+1/A^2} - 1/A\right] . \tag{4.17}$$

Now $\Gamma_V^0/\Gamma_Z^0 \simeq 1.3 \times 10^{-5}$. so we can ignore Γ_V^0 in our analysis, thus $\Delta\Gamma_0 \simeq \Gamma_Z^0$. Using Eqs. (4.11) and (4.8) in Eq. (4.14) we conclude that

$$|A| \leq 0.45 \qquad \text{everywhere} \tag{4.18}$$

therefore

$$\delta\ M_Z - i/2\ \delta\Gamma_Z \simeq m_{VZ}\left[\ \tfrac{1}{2}\ A + 0\left(A^3\right)\ \right]$$

where

$$A = 2m_{VZ}\ \frac{1}{(\Delta M_0 - i/2\ \Delta\Gamma_0)} \quad . \tag{4.19}$$

Finally using

$$\langle V|\mathcal{M}|V\rangle \equiv M_V - i\Gamma_{V/2} \tag{4.20}$$

we conclude that

$$\delta\ M_V - i\delta\Gamma_{V/2} = -\ (\delta M_Z - i\delta\Gamma_{Z/2}) \tag{4.21}$$

where $\delta\ M_V \equiv M_V - M_V^0$ and $\delta\Gamma_V = \Gamma_V - \Gamma_V^0$. In particular

$$\Gamma_V = -\delta\Gamma_Z \simeq \frac{m_{VZ}^2\,\Gamma_Z^0}{\left[(\Delta M_0)^2 + \Gamma_Z^{02}/4\right]} \tag{4.22}$$

The resulting shift of the Z^0 mass and the induced width of the toponium resonance V are shown in Fig. 26. The shift of the Z^0 mass associated with toponium mixing is very small and will not be measured directly in any envisioned collider.

The interference between V and Z^0 will show up in ΔR in the region of the Z^0 pole. Here I will consider only some particular final state $f\bar{f}$ (e.g. $\mu^+\mu^-$) produced in e^+e^- collisions. Define

g_{Vf} - the coupling of the state $|V\rangle$ to the final state $(f\bar{f})$.

and

g_{Zf} - the coupling of the state $|Z\rangle$ to the same final state $(f\bar{f})$.

then

$$\begin{aligned} g_{Vf} &= g_{Vf}^0 \cos\theta - g_{Zf}^0 \sin\theta \\ g_{Zf} &= g_{Zf}^0 \cos\theta + g_{Vf}^0 \sin\theta \end{aligned} \tag{4.23}$$

where g_{Vf}^0 and g_{Zf}^0 are the associated couplings to the unmixed states $|V_0\rangle$ and $|Z_0\rangle$.

The ratio for production of the final state $f\bar{f}$ through the V and Z resonances to the production $\mu^+\mu^-$ through the virtual photon only is given by

(a)

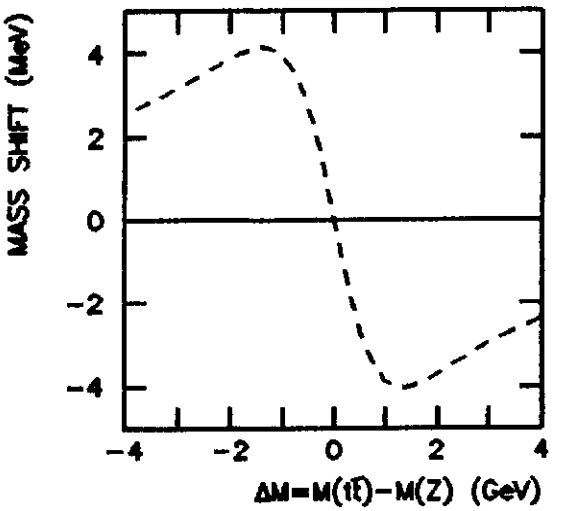

(b)

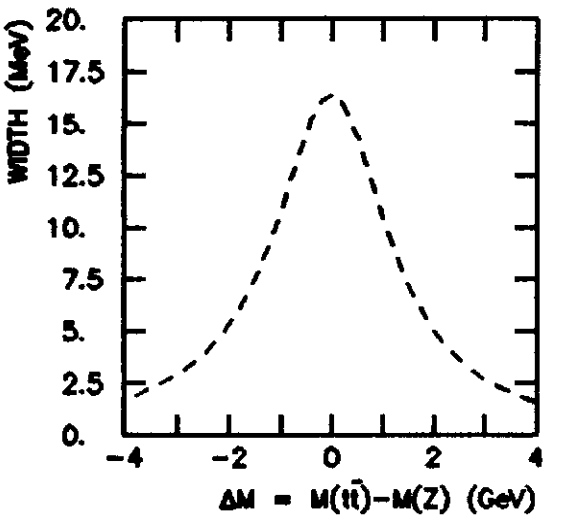

Figure 26: The mass shift (in MeV) of the Z^0 pole (Fig. a) and the induced width (in MeV) of the toponium state V (Fig. b) as a function of the mass difference $\Delta M = m(V_0) - m(Z_0)$ (in GeV).

$$R = s^2\left[\left|\frac{g_{Ve}g_{Vf}}{(s-M_V^2)+i\Gamma_V M_V} + \frac{g_{Ze}g_{Zf}}{(s-M_Z^2)+i\Gamma_Z M_Z}\right|^2\right] . \tag{4.24}$$

Since $\Gamma(V_0 \to \text{all}) \sim 20$ keV we can ignore g^0_{Ve} and g^0_{Vf}. In this limit

$$g_{Vf(e)} \simeq -\sin\theta g^0_{Zf(e)} \text{ and } g_{Zf(e)} \simeq \cos\theta g^0_{Zf(e)} \tag{4.25}$$

so

$$R_f \simeq s^2\left[(g^{0*}_{Ze}g^0_{Ze})(g^{0*}_{Zf}g^0_{Zf})\left|\left(\frac{\sin^2\theta}{s-M_V^2+i\Gamma_V M_V}\right) + \left(\frac{\cos^2\theta}{(s-M_Z^2)+i\Gamma_Z M_Z}\right)\right|^2\right] \tag{4.26}$$

For $e^+e^- \to \mu^+\mu^-$ as an example we have

$$R_\mu = \frac{(L_e^2+R_e^2)(L_\mu^2+R_\mu^2)}{64x_W^2(1-x_W)^2}\left(\left|\frac{\cos^2\theta}{(1-M_Z^2/s)+i\Gamma_Z M_Z/s} + \frac{\sin^2\theta}{(1-M_V^2/s)+i\Gamma_V M_V/s}\right|^2\right) \tag{4.27}$$

To illustrate the interference pattern produced by Eq. (4.27) consider $\Delta M_0 = M_V^0 - M_Z^0 = -1$ GeV; then $\Gamma_V = 10.8$ MeV and $\delta M_Z = 3.9$ MeV. The resulting interference pattern is shown in Fig. 27. In our limit ($\Gamma_V^0=0$) there is an exact zero at $\sqrt{s} = M_V^0$.[53] For $\Delta M_0 = 0$, $\Gamma_V = 16.8$ MeV, $\delta M_Z = 0.0$ and R_μ is shown in Fig. 28. The interference is totally destructive here and a spectacular

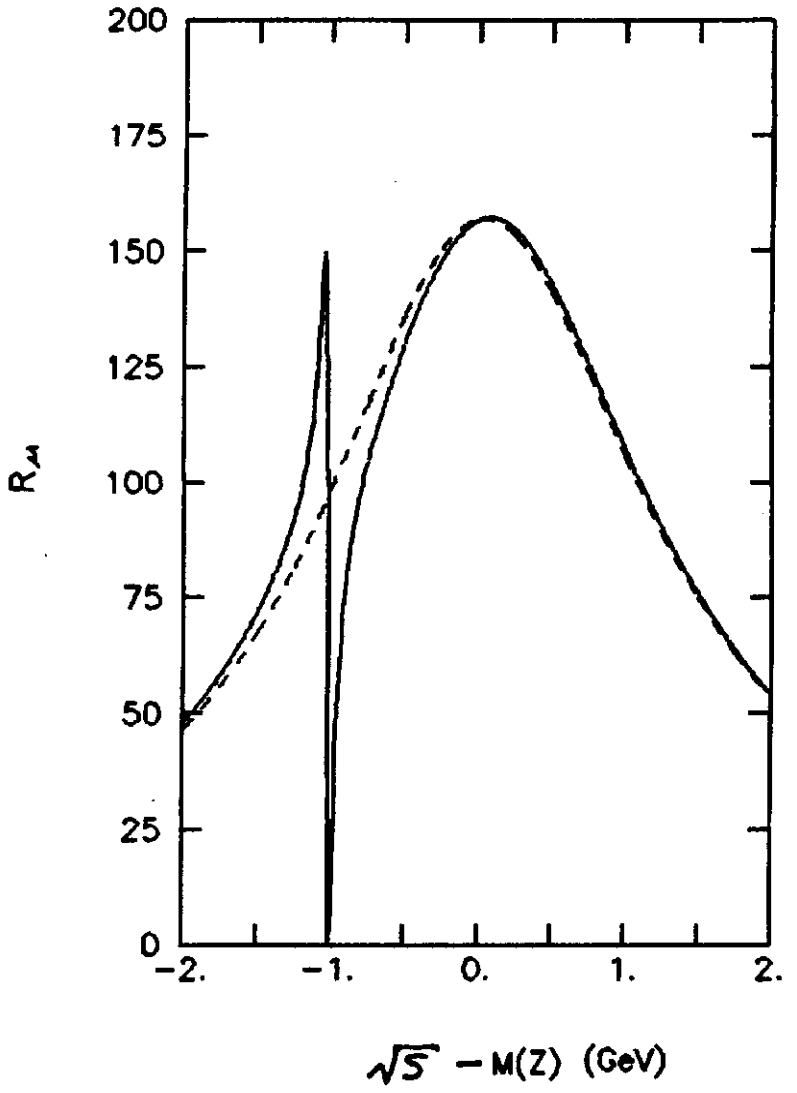

Figure 27: The behaviour of R in the $\mu^+\mu^-$ exclusive channel (R_μ) with a $^3S_1$ toponium resonance in the vicinity of the Z^0 pole. The solid curve is the result when the unshifted mass of the toponium resonance m(V) is chosen to be 1 GeV below the unshifted Z^0 mass m(Z); i.e. the bare mass difference $\Delta M = m(V) - m(Z) = -1$ GeV. The dashed curve shows the R_μ for the Z^0 pole alone. The horizontal axis is $\sqrt{s} - m(Z^0)$ (in GeV), where $\sqrt{s}$ is the center of mass energy of the e^+e^- collider.

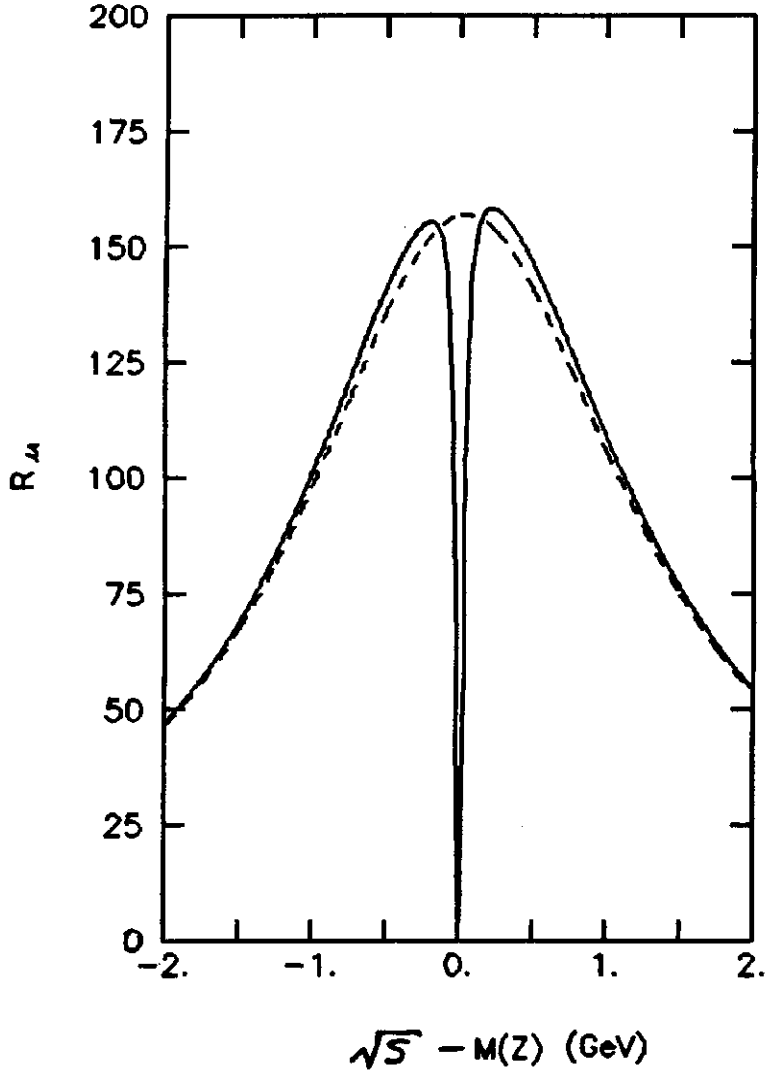

Figure 28: The behaviour of R_μ for $\Delta M = 0$. The toponium state is degenerate in mass with the Z^0. The notation is given in Fig. 27.

narrow dip results. For $\Delta m_0 = +1$ GeV, the pattern is just the reflection about $\Delta m_0 = 0$ of the $\Delta m_0 = -1$ GeV case. The result is shown in Fig. 29. We have not taken account of the experiment resolution. With a $\sqrt{s}$ resolution of 100 MeV most of the structure will be washed out. These matters are discussed in more detail in Ref. (49).

V. SUMMARY

In the standard electroweak model with three generations of fermions only the top quark remains to be discovered. In these lectures I have considered the expected properties of the top system -- both toponium and open top. Emphasis has been placed on what can be learned from the top system about the strong interactions between heavy quarks, i.e. quarkonium physics.

The top quark mass must lie in a range between the experimental lower bound of 22.7 GeV and upper bound of approximately 350 GeV. However for masses above 60 GeV top physics is completely dominated by the weak decay of the top quark. In fact only few lowest toponium states will be observable as distinct resonances. The mass range below 60 GeV is more interesting. It is the transition region between the dominance of strong interaction physics in less massive quarkonium systems and the dominance of electroweak physics in heavier systems. I have concentrated on this mass range. Indeed, the physics for the top mass about one half the Z^0 mass is particulary rich.

The conclusions about quarkonium physics for the top system can

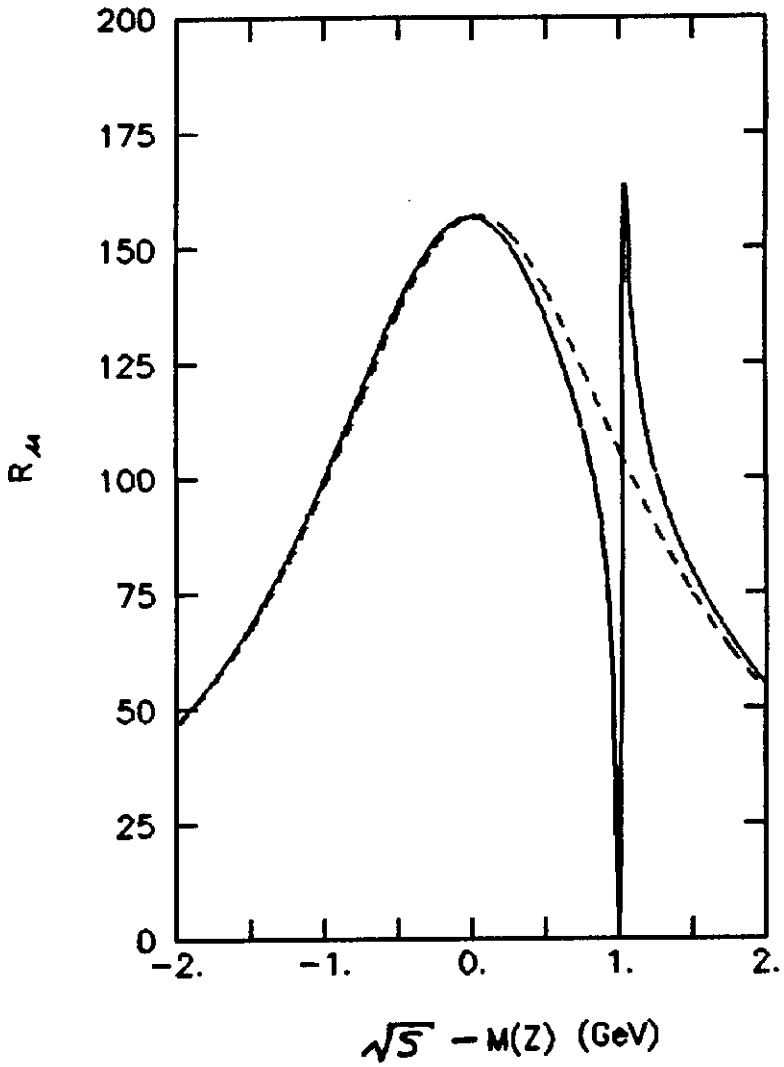

Figure 29: The behaviour of R_μ for $\Delta M = 1$ GeV. The notation is given in Fig. 27.

be organized under the headings of spectroscopy, toponium decays, production of toponium and open top, and exotic physics possibilities.

First let me summarize the results for $(t\bar{t})$ spectroscopy. The spectrum of $(t\bar{t})$ states below threshold is shown in Figure 10 for m_t=45 GeV. Below threshold for Zweig allowed decays, there are 12 S states, orbitally excited states with L as large 17, and in total 424 states. Naively one would expect to learn a great deal about quarkonium physics from this system. However the situation is not as bright as it appears. Some information about the nonrelativistic potential will certainly be obtained -- for example, measuring the 2S - 1S energy splitting should rule out phenomenological potentials which do not have the short distance behavior expected in Q.C.D. But perturbative Q.C.D. alone will not even be sufficient to describe all the properties of the 1S ground state of toponium (for top masses below 60 GeV). Essentially no new information about the relativistic corrections to the potential will be obtained from the top system. The fine and hyperfine splittings of low-lying multiplets will be dominated by the perturbative contribution. Hence the long range part of the spin dependent forces will not be tested. Even more discouraging is the fact that the total fine structure splittings in the 1P states are so small as to be experimentally unobservable.

In the decays of toponium states the emergence of electroweak physics become clear as the top quark mass increases. The decays of the $^3S_1$ $(t\bar{t})$ ground state are shown in Figure 14. Near the Z^0 mass

the decays are dominated by virtual Z^0 decays and above this mass by weak top decays. For excited states the situation, shown in Figure 16, is the same. Since the direct decays dominate for $m_t > 40$ GeV the other J^{PC} $(t\bar{t})$ states become inaccessible via transitions from excited S states.

The production in e^+e^- collisions of the 1^3S_1 $(t\bar{t})$ ground state resonance should be observable for any top quark mass within the kinematically assessible energy range at LEPI. However the situation for excited states is more complicated. The electronic widths decrease rapidly with increasing radial quantum number. Already, $\Delta R_{peak} < 2$ for the 3 S state (except very near the Z pole). Furthermore with the resolution expected at SLC it will be problematic to resolve separate $^3S_1$ state resonances near threshold since the spacing between successive states will only be about 80 MeV. Above threshold the toponium states will decay into open top mesons. The hyperfine splittings between the pseudoscalar (T) and vector (T*) open top states is so small that it is comparable to the electroweak mass difference between the charged and neutral states. This is shown in Figure 20. Both the T* and the T will decay weakly. The M1 transition between the T* and T has an unobservably small branching ratio. Because the experimental energy resolution is comparable to the natural width of toponium states above threshold, the usual distinction between narrow states below and wide states above threshold will be blurred.

Finally a few exotic possibilities have been considered. If there is a charged Higgs scalar with a mass sufficiently below the

top mass then the semiweak decay of the top quark into this charged Higgs boson and a bottom quark will dominate the $(t\bar{t})$ decays. The more conventional neutral Higgs can be observed via the Wilczek mechanism for masses up to 60 GeV with a 1 S $(t\bar{t})$ state of mass 75 GeV. Near the Z^0 mass there can be direct production of $^3P_1$ $(t\bar{t})$ states at an observable rate. This production is due to the axial vector couplings of the Z^0. Most interestingly, if the toponium system is very close to the Z^0 mass interference effects can be large. This results in an induced width of the 1^3S_1 toponium resonance of approximately 20 MeV (see Figure 26), and some spectacular effects in R. Some examples of the effects in R of mixing of a single 1^3S_1 toponium resonance with the Z^0 are shown in Figures 27-29.

The top system is the last hurrah for standard quarkonium physics in two distinct senses. First, of course, within the standard model with three generations the top quark is the only remaining quark system. But also the top system with $m_t \lesssim 60$ GeV is at the boundary between the dominance of ordinary strong interaction physics (Q.C.D.) and electroweak interaction physics. As the mass increases the toponium resonances decay increasingly via weak decays of the top quark. This leads to large widths which will eventually smear out the distinct resonances. Also the branching ratios for transitions from excited S states to $(t\bar{t})$ states with other J^{PC} become unobservably small. So also in this second sense the top system is the last hurrah for standard quarkonium physics.

References and Footnotes

[1] M. E. Peskin, Proc. 1983 SLAC Summer Institute of Particle Physics, Edited by P. McDonough, SLAC Report No. 267 (1983), pgs. 151-190.

[2] The one loop result was first obtained by A. Duncan, Phys. Rev. D13, 2866 (1976).

[3] The two loop result has been calculated by: F.L. Feinberg, Phys. Rev. Lett. 39, 316 (1977); T. Appelquist, M. Dine, and I. Muzinich, Phys. Lett. 69B, 231 (1977); and W. Fischler, Nucl. Phys. B129, 157 (1977).

[4] W.E. Caswell, Phys. Rev. Lett. 33, 244 (1974).

[5] W. Buchmuller and S.-H. H. Tye, Phys. Rev. D24, 132 (1981).

[6] E. Eichten et. al., Phys. Rev. D17, 3090 (1979); D21, 203 (1980).

[7] J. Richardson, Phys. Lett. 82B, 272 (1979). For an extension of this model see Ref. 5.

[8] A. Martin, Phys. Lett. 93B, 338 (1980).

[9] C. Quigg and J. Rosner, Phys.Lett. 71B, 153 (1977).

[10] C. Quigg, H.B. Thacker, and J. Rosner, Phys. Rev. D18, 274 (1978); Phys. Rev. D18, 287 (1978); Phys. Rev. D21, 234 (1981).

[11] C. Quigg and J. Rosner, Phys.Rev. D23, 2625 (1981).

[12] For a general review of lattice methods in Q.C.D. see for example: Quarks, Gluons, and Lattices, M. Creutz, Cambridge Monographs on Mathematical Physics, University Press, 1983 (Cambridge, UK) p.169

[13] S. Otto and J. Stack, Phys. Rev. Lett. 52, 2328 (1984).

[14] D.D. Barkai, K.J.M. Moriaty, and C. Rebbi, Phy. Rev. D30, 1293 (1984).

[15] A. Hasenfratz and P. Hasenfratz, Phys.Lett. 93B, 241 (1980). The relation between Λ_{MOM} and $\Lambda_{\overline{MS}}$ was computed by W. Celmaster and R. J. Gonsalves, Phy. Rev. D20, 1420 (1979).

[16] For a discussion of this point see: E. Eichten, Proc. 1983 SLAC Summer Institute of Particle Physics, Edited by P. McDonough, SLAC Report No. 267 (1983), pgs. 497-516; and references therein.

[17] This limit is obtained by using the expected properties of the lowest $^3S_1$ toponium state in the Richardson potential. In particular, the ground state is expected to be 1.15 GeV below threshold for Zweig allowed decays (for a top quark mass at the lower bound given in Eq. 2.1) and the relation between the mass of the top quark and the ground state open top meson discussed in the text ($m_t = M_T - .43$ GeV). Then the reported limit on narrow charge 2/3 ($Q\bar{Q}$) resonances (M. Althoff et.al., Phys. Lett. 138B, 441 (1984)) of $M(Q\bar{Q}) > 45.2$ GeV can be converted into the limit shown.

[18] W.J. Marciano and A. Sirlin, Phys. Rev. D29, 75 (1984).

[19] C. Rubbia, Seminar at the 1984 Summer Study of the Design and Utilization of the Superconducting Super Collider, (Snowmass, Colorado).

[20] C. Quigg and J. Rosner, Phys. Report 56C, 167 (1979).

[21] W. Buchmuller, "Testing Q.C.D. In Quarkonium Spectroscopy",

presented at the Moriond Workshop on New Flavors, Les Arcs, France, Jan. 24-30, 1982.

[22] For some examples of the dependence of the ground state properties on the intermediate distance behaviour for more complicated phenomenological potentials see: H. Krasemann and S. Ono, Nucl. Phys. B154, 283 (1979).

[23] E. Eichten, Phy. Rev. D22, 1819 (1980).

[24] E. Eichten and F. Feinberg, Phy. Rev. Lett. 43, 1205 (1979); Phy. Rev. D23, 2724 (1981).

[25] D. Gromes, Z. Phys. C26, 401 (1984).

[26] W. Buchmuller, Phys. Lett. 112B, 479 (1982). This form is also predicted in the context of the MIT Bag Model: K. Johnson (unpublished); and J. Baake, Y. Igarashi, and G. Kasperidus, Z. Phys. C9, 203 (1982).

[27] J. Gaiser, "Charmonium Spectroscopy From the Radiative Decays of the J/ψ and ψ' ," Ph. D. Thesis, Stanford University, SLAC-PUB 255 (1982).

[28] For a more extensive discussion of these points see: D. Gromes, "Ordinary Hadrons", Lectures given at the Yukon Advanced Study Institute, Whitehead, Yukon, August 11-26, 1984; Heidelberg preprint HD-THEP-84-21(1984).

[29] W. Buchmuller, Y.J. Ng, and S.-H. H. Tye, Phy. Rev. D24, 3003 (1981).

[30] P. M. Tuts, "Heavy Quarkonia", Summary talk presented at the International Symposium on Lepton and Photon Interactions at High Energies, Cornell University, August 4-9, 1983.

[31] I.I.Y. Bigi and H. Krasemann, Z. Phys. C7, 127 (1981).

[32] L.M. Sehgal and P.M. Zerwas, Nucl. Phys. B183, 417 (1981).

[33] J. Leveille, Proceedings of the Cornell Z Workshop, February 6-8, Ithaca (1981), Edited by M. Peskin and S.-H. H. Tye, CLNS-81/485, p.241.

[34] J.H. Kuhn and K.H. Streng, Nucl. Phys. B198, 71 (1982) and the references contained therein.

[35] See for example the charmonium review of T. Appelquist, R.M. Barnett, and K.D. Lane, Ann. Rev. Nucl. Sci. 28, 387 (1978).

[36] Y.P. Kuang and T.-M. Yan, Phy. Rev. D24, 2874 (1981).

[37] This table and the discussion of the radiative corrections to R are taken with minor modifications from: J.D. Jackson, S Olsen, and S.-H. H. Tye, in the Proceedings of the 1982 Summer Study on Elementary Particles and Fields, Snowmass, edited by R. Donaldson, R. Gustafson, and F. Paige (Amer. Inst. Phys., N.Y., 1983), pg.175.

[38] A. Barbaro - Galtieri, in the Proceedings of the 1977 International Symposium on Lepton and Photon Interactions at High Energies, August 25-31, Hamburg (1977), Edited by F. Gutbrod, pg. 21.

[39] D. Besson et. al., Phy. Rev. Lett. 54, 381 (1985). Similar structure has also been observed by D.M.J. Lovelock et. al., Phy. Rev. Lett. 54, 377 (1985).

[40] More extensive discussions of the behaviour of R in the threshold region of top production have appeared after these lectures were presented. See S. Gusken, J.H. Kuhn, and P.M.

Zerwas, CERN Preprint CERN-TH.4106/85 and Ref. 49. Also see R.A. Berltmann and S. Ono, Z. Phys. C8, 271 (1981).

[41] D. Kreinick, in these proceedings.

[42] Near the Z^0 pole the axial vector coupling of the Z^0 will produce different relative couplings to pseudoscalars and vector open top mesons. However these couplings are strongly suppressed due to their P wave nature. See the first citation in Ref. 37 and also my discussion of direct production of P states given in Section 4.

[43] K.D. Lane and S. Weinberg, Phy. Rev. Lett. 17, 717 (1976).

[44] M. Aguilar-Benitez et. al., (Particle Data Group), Phys. Lett. 111B (1982).

[45] For a general discussion of the scalar sector of the Electroweak Interactions see: K.D. Lane, in the Proceedings of the 1982 Summer Study on Elementary Particles and Fields, Snowmass, edited by R. Donaldson, R. Gustafson, and F. Paige (Amer. Inst. Phys., N.Y., 1983), pg. 222.

[46] F. Wilczek, Phy. Rev. Lett. 39, 1304 (1977).

[47] J.H. Kuhn and S. Ono, Z. Phys. C21, 395 (1984).

[48] I thank F. Gilman for pointing out the factor of $\sqrt{3}$ which I had missed in my SLAC Summer School Lectures.

[49] P. Franzini and F. Gilman, SLAC Preprint, SLAC-PUB-3541 (1985).

[50] J.H. Kuhn and P.M. Zerwas, CERN Preprint, CERN-Th.4089/85 (1985).

[51] F.M. Renard, Z. Phys. C1, 225, (1979).

[52] Since the states are resonances with significant decay widths the S Matrix including these resonances is not unitary. In the present discussion this implies that the complex angle in Eq. (4.12) should not be complex conjugated when the states $\langle Z|$ and $\langle V|$ are constructed from $|Z\rangle$ and $|V\rangle$.

[53] This was first realized by the authors of Refs. 49 and 50. The graphs originally presented in my lectures were incorrect.